Pacific Northwest
NATIONAL LABORATORY

PNNL-32000

An Investigation of Strategies for Sensing Window Attachment Position: Survey of Candidate Technologies, Evaluation, and Deployment Recommendations

September 2021

TJ Pilet
WE Hunt

U.S. DEPARTMENT OF ENERGY

Prepared for the U.S. Department of Energy
under Contract DE-AC05-76RL01830

DISCLAIMER

This report was prepared as an account of work sponsored by an agency of the United States Government. Neither the United States Government nor any agency thereof, nor Battelle Memorial Institute, nor any of their employees, makes **any warranty, express or implied, or assumes any legal liability or responsibility for the accuracy, completeness, or usefulness of any information, apparatus, product, or process disclosed, or represents that its use would not infringe privately owned rights**. Reference herein to any specific commercial product, process, or service by trade name, trademark, manufacturer, or otherwise does not necessarily constitute or imply its endorsement, recommendation, or favoring by the United States Government or any agency thereof, or Battelle Memorial Institute. The views and opinions of authors expressed herein do not necessarily state or reflect those of the United States Government or any agency thereof.

PACIFIC NORTHWEST NATIONAL LABORATORY
operated by
BATTELLE
for the
UNITED STATES DEPARTMENT OF ENERGY
under Contract DE-AC05-76RL01830

Printed in the United States of America

Available to DOE and DOE contractors from
the Office of Scientific and Technical Information,
P.O. Box 62, Oak Ridge, TN 37831-0062
www.osti.gov
ph: (865) 576-8401
fox: (865) 576-5728
email: reports@osti.gov

Available to the public from the National Technical Information Service
5301 Shawnee Rd., Alexandria, VA 22312
ph: (800) 553-NTIS (6847)
or (703) 605-6000
email: info@ntis.gov
Online ordering: http://www.ntis.gov

An Investigation of Strategies for Sensing Window Attachment Position: Survey of Candidate Technologies, Evaluation, and Deployment Recommendations

September 2021

TJ Pilet
WE Hunt

Prepared for
the U.S. Department of Energy
under Contract: DE-AC05-76RL01830

Pacific Northwest National Laboratory
Richland, Washington 99352

Abstract

While windows are desirable feature in buildings for views, daylighting, and aesthetics, it is important to recognize that windows are a major contributor to a building's energy load. Interior window coverings, such as shades and blinds, can help improve the energy performance of windows without sacrificing the benefits; however, while appropriate use of window coverings provide the potential for energy savings, there is little consensus regarding how occupants typically use these window attachments, which sometimes puts into question how much energy they actually save in an occupied home. Automated shading control strategies can reduce the uncertainty of energy savings; however, users can overwrite pre-defined schedules or write their own shade control programs to reach their personal comfort and privacy goals. Because it is difficult to identify how occupants interact with window shades, it is difficult to identify the energy savings potential of blinds.

To address this problem, this study was developed to identify a candidate sensor that can be deployed to sense blind position. The intended application for this sensor is deployment in energy efficiency field studies so that shade usage can be measured to better understand results and identify the energy impact of specific window attachment technologies.

Summary

While appropriate use of window coverings provides the potential for energy savings, there is little consensus regarding how occupants typically use window attachments[1], which sometimes puts into question how much energy they save in an occupied home. Automated shading control strategies can reduce the uncertainty in energy savings, but users can overwrite the pre-defined schedules or write their own shade control programs to reach their personal comfort and privacy goals, thereby reintroducing a factor of uncertainty in the energy impact of window attachments. Because it is difficult to identify how occupants interact with window shades during field studies, it is difficult to identify the energy savings potential of blinds.

This study was developed to identify add-on sensing strategies that can be deployed to capture the blind position in field studies. The intended application for this sensor is deployment in occupied field settings, so that use of the shades can be measured to better understand results and identify the energy impact of specific window attachment technologies. This study comprised many tasks that built upon each other and motivated testing selections and final recommendations. A flowchart outlining the project tasks and their specific outcomes is provided in Figure S.1.

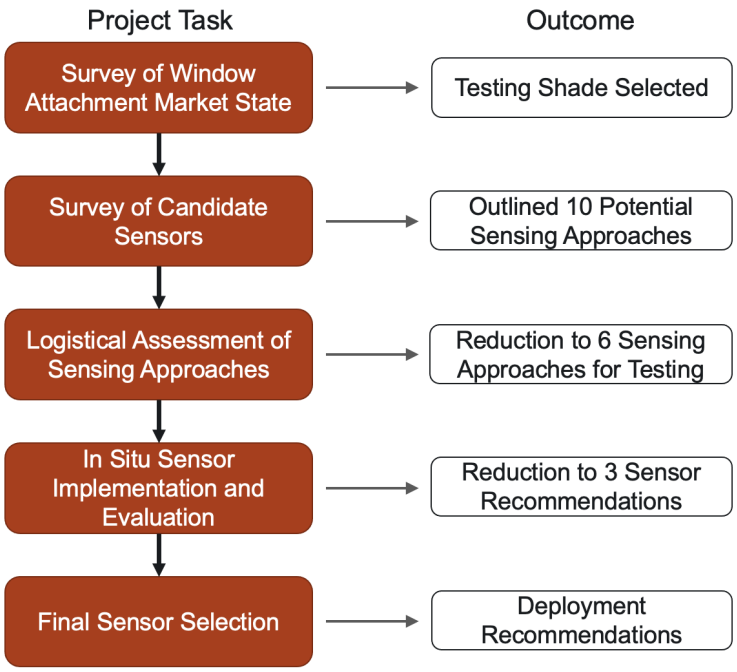

Figure S.1. Task groupings and their specific outcomes throughout this project.

[1] Cort, K. A., McIntosh, J. A., Sullivan, G. P., Ashley, T. A., Metzger, C. E., & Fernandez, N. (2018). Testing the Performance and Dynamic Control of Energy-Efficient Cellular Shades in the PNNL Lab Homes. https://doi.org/10.2172/1477792.
Foster, M., & Oreszczyn, T. (2001). Occupant control of passive systems: the use of Venetian blinds. Building and Environment, 36(2), 149–155.
Van Den Wymelenberg, K. (2012). Patterns of occupant interaction with window blinds: A literature review. Energy and Buildings, 51, 165–176.

In Figure S.1, the broad groupings of tasks within this project are displayed, along with their outcomes, which drove subsequent tasks. At the start of this project, a preliminary study was conducted to place the state of the window attachments market in context. The focus of this study was to contextualize this project and its potential impact, while also identifying a window attachment upon which to base all testing. This market survey found that 62% of window attachments in the American residential market are blinds, and 44% of all window attachment types are horizontal Venetian blinds[2]. (Bickel et al., 2013). This finding resulted in the selection of a Venetian blind for sensor testing and implementation. After this, a survey identified candidate sensors and resulted in the discovery 10 potential sensing approaches. After a preliminary screening based on sensor compatibility and installation, these sensors were paired down to six position-sensing approaches that were installed and tested. Following testing, the six tested sensors were reduced to three recommended sensors, based upon the testing results and lessons learned during implementation. The six tested sensing techniques, along with their estimated material costs and scoring of implementation effort, are tabulated below

Table S.1.Summary of sensor testing results.

Sensor Type	Sensor Model	Raw Material Cost ($)	Implementation Effort (Qualitative Assessment)
Sill-Mounted Ultrasonic Distance Sensor	HC-SR04	$6.75	Low
Shade-Mounted Ultrasonic Distance Sensor	HC-SR04	$7.06	Medium
Sill-Mounted Infrared Distance Sensor	VL53L0X	$11.75	Low
Shade-Mounted Infrared Distance Sensor	VL53L0X	12.06	Medium
Hall Effect Sensor Array	A3144	$18.78	High
Magnetic Encoder Strip	A3144/Adafruit #4680	$101.55	High

The candidate sensors listed in Table S.1 were installed on a horizontal Venetian blind for testing. During the testing, the shade was actuated to prescribed locations spaced 6 inches apart along the shade's vertical travel of 60 inches. Sensor outputs were measured against reference measurements in two trials: (1) immediately after installation and (2) after 24 hours in service on a shade that was actuated 10 times. These two tests were designed to simulate sensor deployment in an energy efficiency field study. The experimental testing results for each of the candidate sensing strategies are presented in Table S.2.

[2] Bickel, S., Phan-Gruber, E., & Christie, S. (2013). Residential Windows and Window Coverings: A Detailed View of the Installed Base and User Behavior. In US Department of Energy Office of Energy Efficiency and Renewable Energy. https://www.energy.gov/sites/prod/files/2013/11/f5/residential_windows_coverings.pdf

Table S.2. Summary of sensor testing results.

Sensor Type	Post-Installation Mean Error (%)	Mean Error after 24-Hours in Service (%)	General Performance Rating
Sill-Mounted Infrared Distance Sensor	9.33%	14.0%	Acceptable
Shade-Mounted Infrared Distance Sensor	46.6%	99.9%	Unacceptable (due to repeatability issues)
Sill-Mounted Ultrasonic Distance Sensor	1.26%	1.93%	Acceptable
Shade-Mounted Ultrasonic Distance Sensor	4.26%	21.1%	Unacceptable (due to repeatability issues)
Hall Effect Sensor Array	18.3%	18.3%	Acceptable (due to strong repeatability)
Magnetic Encoder Strip	5.70%	160%	Unacceptable (due to compounding error)

Based upon the testing results and lessons learned from the implementation of each of the sensors, three candidate sensors separated themselves from the rest: the sill-mounted ultrasonic distance sensor, the sill-mounted infrared distance sensor, and the Hall effect sensor array. The infrared and ultrasonic distance sensors are functionally equivalent from an implementation standpoint, but the ultrasonic distance sensor outperformed the infrared distance sensor in the experimental testing of this study. Because of this performance gap, the infrared distance sensor was disregarded in favor of the remaining two recommended sensors—the ultrasonic distance sensor and the Hall effect sensor array. These two sensors have very different inner workings and implementations, thus lending themselves better to deployment on different shade types. A summary of deployment recommendations for various shade types is presented in Table S.3. For more detailed deployment recommendations, detailed descriptions of sensor implementation for various shade types are presented in Section 7.0.

Table S.3 Summary of sensor deployment recommendations by shade type.

Shade Type	Recommended Sensor	Details of Implementation Recommendation
Venetian Blinds	Ultrasonic, Sill-Mounted	See Section 7.1
Roller Shades	Hall Effect Sensor Array	See Section 7.3
Vertical Blinds	Ultrasonic, Frame-Mounted	See Section 7.2
Cellular Shades	Ultrasonic, Sill-Mounted	See Section 7.4

Shade Type	Recommended Sensor	Details of Implementation Recommendation
Roman Shades	Hall Effect Sensor Array	See Section 7.4
Sheer Shades	Ultrasonic, Sill-Mounted	See Section 7.4

For field deployment, certain sensors are better suited to sensing certain types of shades. Ultrasonic distance sensors are well-suited for measuring the position of shades that have thicker depths. The Hall effect sensor array is better suited for shades that may have thinner bottom rails, which may be difficult for an ultrasonic sensor to target. Another benefit of these two recommended sensors is their low cost. The ultrasonic distance sensor is an off-the-shelf product that can be acquired and deployed for approximately $8 per shade, and the Hall effect sensor comprises parts that cost approximately $20 per shade. This study and its recommendations address a gap in the area of window attachments performance testing and field validation. Utility energy efficiency programs in need of measures that feature verifiable and persistent energy savings, and manufacturers that want to validate the energy-saving capabilities of their products, could both benefit from the application of these sensors and evaluation strategies in utility pilot studies. This study addresses this need and sets the foundation for future research on the energy impact of window shades.

Acknowledgments

The project team thanks Katherine Cort, Patricia Gunderson, Jaime Kolln, Edward Louie, and Samuel Rosenberg from PNNL for their input on sensor selection and experiment design. Special thanks also goes to Stephen Mullaly of Hunter Douglas for his advice on sensor design, sensor interfacing, and shade selection for this study.

We also thank Susan Ennor and Katherine Cort of PNNL for editorial assistance with this report.

Finally, the authors thank the Buildings Technology Office of the U.S. Department of Energy (DOE) for sponsoring this work, with a special thanks to Marc LaFrance at DOE for his guidance and recommendations.

Acronyms and Abbreviations

ADC	analog-to-digital converter
AERC	Attachment Energy Rating Council
DOE	U.S. Department of Energy
EPA	U.S. Environmental Protection Agency
I^2C	Inter-Integrated Circuit (Communication)
IR	infrared
SPI	Serial Peripheral Interface
WCMA	Window Covering Manufacturers Association

Table of Contents

Table of Figures

Table of Tables

1.0 Introduction

In 2020, residential buildings used approximately 6.17 quadrillion Btu for cooling and heating, with space conditioning loads making up approximately 54.3% of that energy use (EIA 2021). Thermal losses through windows make up a large portion of this usage, as it is estimated that approximately 25% of energy losses in buildings occur via windows (Huang, Hanford, and Yang 1999). While windows are desirable in buildings for views, daylighting, and aesthetics, it is important to recognize that they are a major contributor to a building's energy load. Appropriate use of interior shades and blinds can help enhance the positive aspects of windows while minimizing thermal losses and unwanted thermal gains (Rubin, Collins, and Tibbott 1978; Petersen et al. 2016; Cort et al. 2018). Appropriate use of interior shades and blinds can enhance comfort and reduce unwanted thermal gains. When used appropriately, thermally insulated shades offer a unique opportunity to improve the thermal performance of windows year-round without the need for costly retrofitting or replacement.

While blinds do provide the potential for energy savings, there is little consensus regarding occupant use of blinds (Van Den Wymelenberg 2012; Foster and Oreszczyn 2001). Individuals tend to fall into one of three groups: those who leave blinds open at all times, those who leave blinds closed at all times, and those who modulate blind position throughout the day (Bavaresco and Ghisi 2018). Because of these differences in operation, it is difficult to identify how shades are used in buildings. This discrepancy can potentially be addressed with the inclusion of automated blinds, which modulate based on light levels or a programmed schedule; however, users can readily overwrite the pre-defined shade controls to reach their personal comfort goal. Regardless of whether shade control or automation is implemented, it is difficult to identify how occupants interact with window shades, making it quite difficult to identify the true savings potential of blinds for individual use cases.

The research reported here aims to establish an approach to measuring the shade position of in-service blinds for field studies. At this time, few technologies are available to measure shade position. Those that do exist tend to be proprietary technologies customized to individual automated shade assemblies. The goal of this work is to identify a candidate sensing technology that can be broadly applied to shades of different typologies and constructions, rather than a narrow application on a specified shade type. This work sets the foundation for future work to package and deploy the identified sensor, or combination of sensors, in the field to better understand the impact of shade position and control.

The ensuing chapters of this report describe the status of the window attachment market, present a survey of potential sensing technologies to sense shade position, and provide detailed implementation instructions, an evaluation of sensor performance, and recommendations for field deployment. This study is designed to be a reference for those designing and implementing energy efficiency studies for the study of window attachments' performance and operation.

2.0 Background

To provide context for subsequent sections of this report, this section provides background information about relevant windows, window attachments, and the selection of candidate window attachments for field application.

2.1 Window Component Terminology

Windows are a complex component of building envelopes. Windows serve to connect the interior of a building to the exterior of a building via a punched opening in the opaque building envelope. Due to the thickness of an opaque façade compared to that of an envelope, windows comprise many pieces that serve as mechanical connections between both envelope components. The many components of a typical window are shown in Figure 2.1, which is meant to serve as a guide for the window components referenced in subsequent sections and chapters of this report.

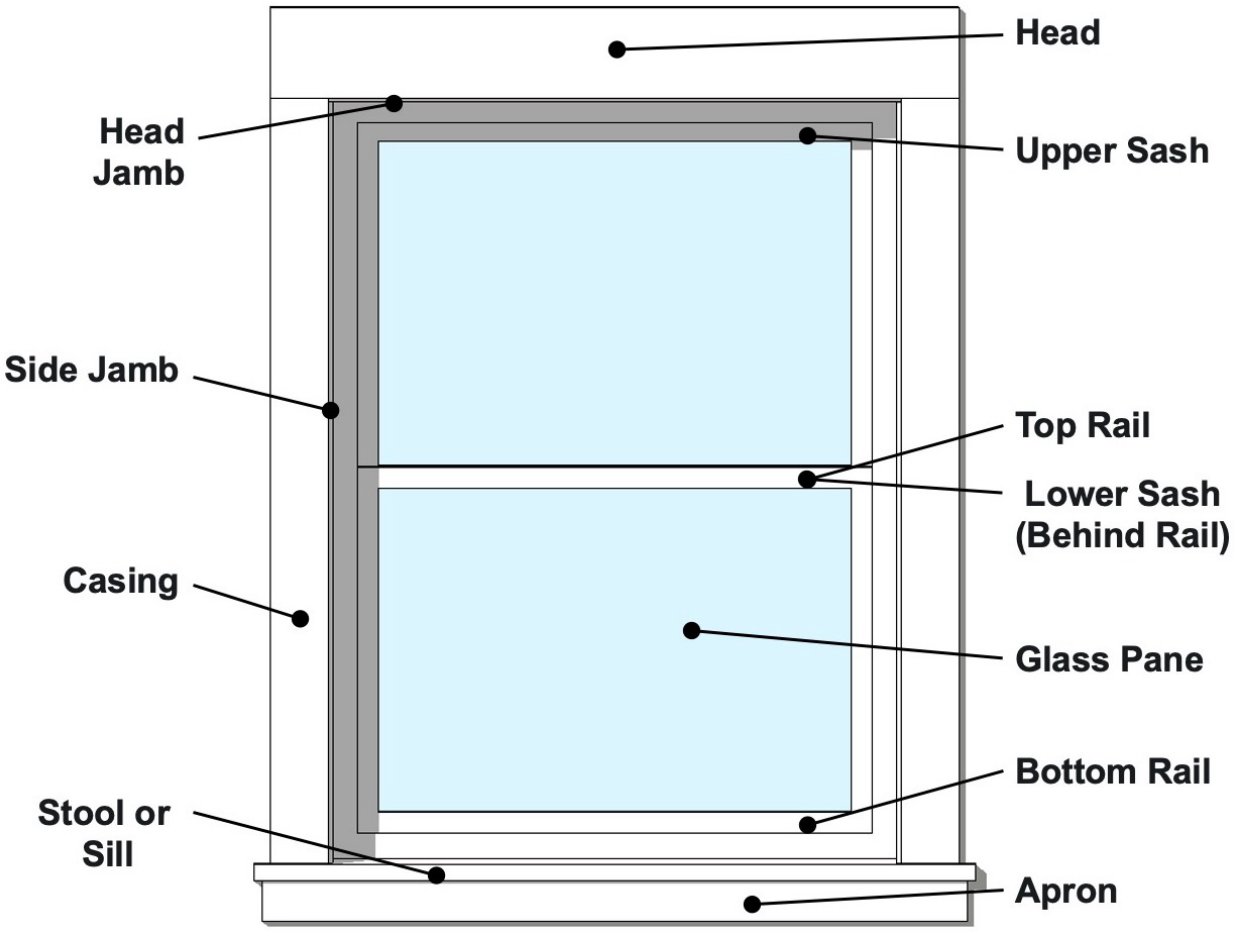

Figure 2.1. Anatomy of a typical window assembly.

2.2 State of the Window Attachment Market

The state of window attachments in the American market is diverse. While most consumers typically envision blinds when hearing the term window attachments, the window attachment

space is broad: curtains, shades, shutters, and blinds are all categorized as window attachments. To better understand the state of window attachments in the United States, the U.S. Department of Energy (DOE), US Environmental Protection Agency (EPA), and the Window Covering Manufacturers Association (WMCA) sponsored research in 2013 to characterize the state of the American window and window attachment market space (Bickel, Phan-Gruber, and Christie 2013). Many of this study's findings provide context and motivation for this work.

In 2015, the DOE sponsored the development of the Attachment Energy Rating Council (AERC), which is an independent, public interest, non-profit organization whose mission is to rate, label, and certify the energy performance of window attachments, such as interior shades and blinds. Each product rated by the AERC includes performance metrics related to its insulating, solar control, and air-leakage features, associated with based on assumed "average use". Operational settings based on the findings of Bickel et al. (2013). In 2020, cellular shades received the first AERC energy rating for an interior shade. As the AERC explores options to characterize the enhanced energy performance associated with optimal control and automation, more data about shade operation settings in the field will help quantify the benefits of this feature and inform consumers about how best to achieve maximum savings from a given product.

The residential market distribution of the different categories of interior window attachments based on Bickel et al. (2013) is shown in Figure 2.2.

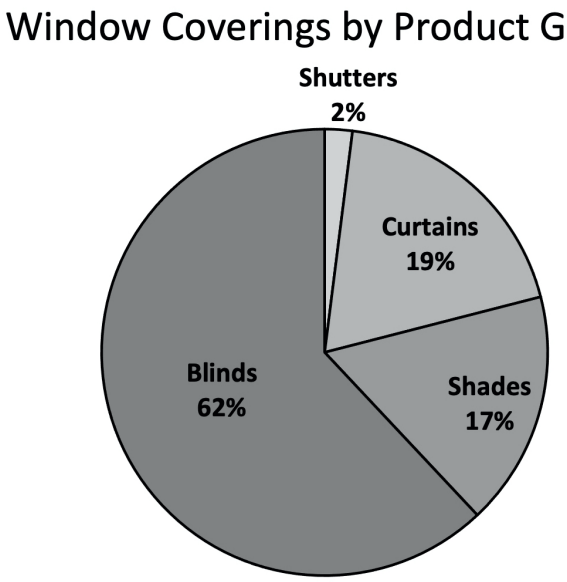

Figure 2.2. Window attachment market space by product grouping (Bickel, Phan-Gruber, and Christie 2013).

From Figure 2.2, it can be concluded that the most prevalent interior window attachment group in the American residential market is blinds, which compose 62% of the market. Because of their function and placement, shades can also be grouped with blinds, and together they compose 79% of the window attachment market.

This distribution of window attachments can also be analyzed by window attachment type. The market study defines attachment types as more specific delineations of window attachment

type; for example, the types of window attachments are cellular shades, roller shades, or horizontal blinds as opposed to generic groupings of shades or blinds. This breakdown of the market space allows for a more specific characterization of prevalent blind technologies, which is important for the design of research like this work. The full breakdown of the residential window attachment market space presented by attachment type is shown in Figure 2.3.

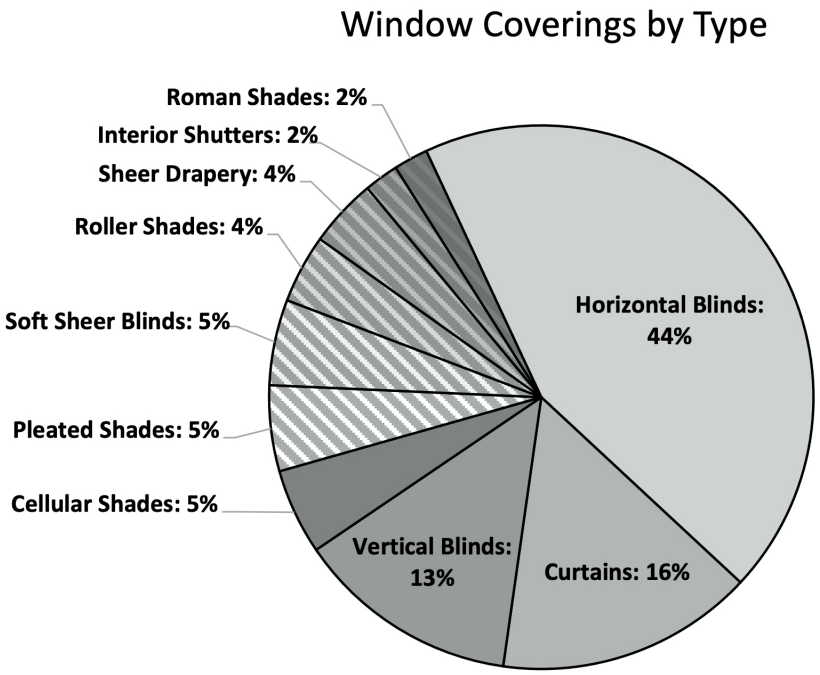

Figure 2.3. Window attachment market space by product typology (Bickel, Phan-Gruber, and Christie 2013).W

Of all of the categories displayed, horizontal blinds, or Venetian blinds, are at the forefront of the window attachment market with 44% of the residential market share.

In addition to the window attachment type, the window attachment mounting location is also an impactful factor in the design of window attachment sensing technologies. Most window attachment mounting styles can be described as “inside mount” or “outside mount” styles, depending on the mounting location in relation to the window assembly. The inside-mount mounting location describes window attachments affixed to the head jamb of a window, and the outside-mount mounting location describes window attachments affixed to the head casing of a window assembly. These mounting styles are graphically represented in Figure 2.4.

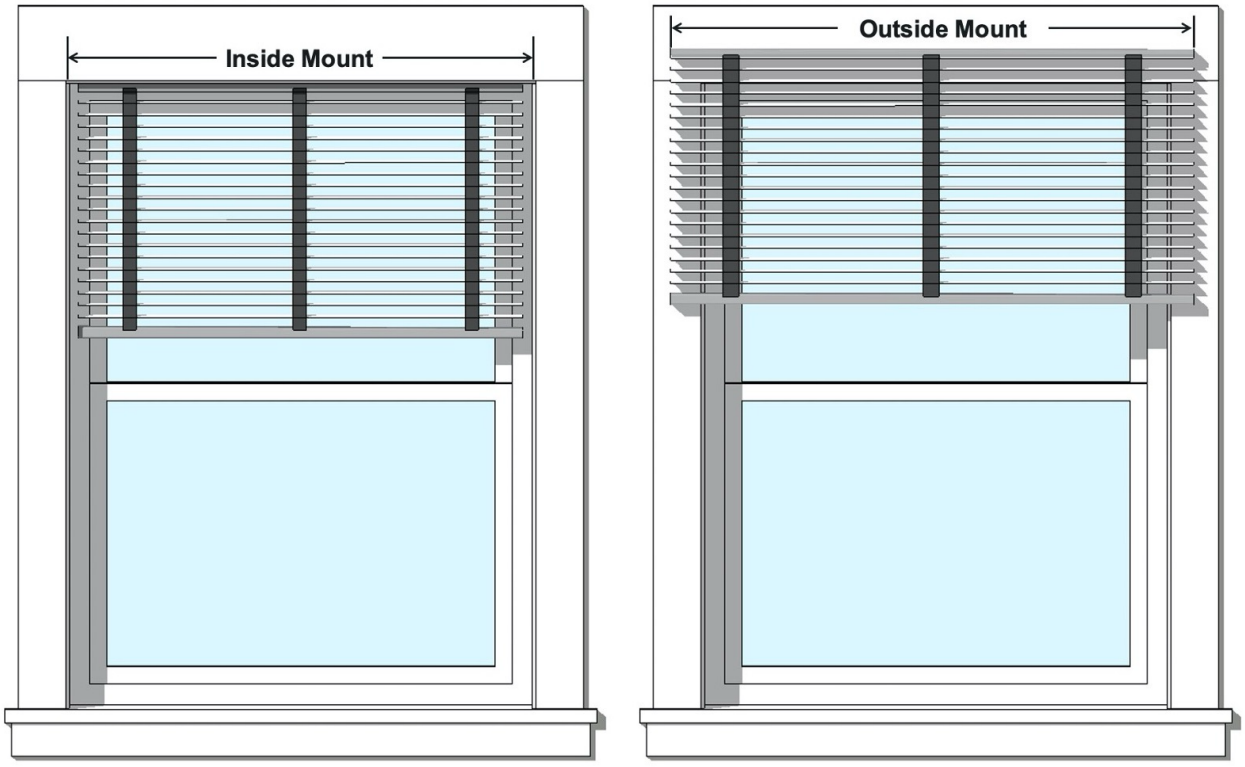

Figure 2.4. Window attachment mounting positions: (a) inside mount (b) outside mount.

With these two mounting positions, the report by Bickel et al. (2013) surveyed the mounting location of all typical window attachment types. These results are summarized in Table 2.1.

Table 2.1. Window attachment mounting styles (Bickel, Phan-Gruber, and Christie 2013).

	Mount Type (%)	
Covering Type	Inside Mount	Outside Mount
Horizontal Blinds	80.4	19.6
Curtains	25.6	74.4
Vertical Blinds	59.6	40.4
Cellular Shades	74.7	25.3
Pleated Shades	79.2	20.8
Roller Shades	73.6	26.4
Sheer Drapery	32.1	67.9
Soft Sheer Blinds	72.0	28.0
Interior Shutters	60.2	39.8
Roman Shades	67.9	32.1

Table 2.1 lists the distribution of mounting locations for different window attachments. Note that the majority of blinds, shades, and shutters tend to be inside mounted, meaning that they are mechanically affixed to the head jamb of the window assembly. Drapery and curtains tend to be

outside mounted on the head casing of window assemblies. Based on the market data presented in Figure 2.2 and Figure 2.3, it can be concluded that the configuration and operation of a horizontal Venetian blind mounted on the window head jamb would be a reasonable representation of a “typical” home’s window covering in the U.S. This information can be used to develop a baseline window attachment that represents a majority of residential window attachments for window attachment sensing applications.

2.3 Blind Component Terminology

Leveraging market statistics from Section 2.2, it can be concluded that horizontal Venetian blinds are the most common window attachment found in American households. With the prevalence of this window attachment typology known, it is important to identify the conventions for naming the various window shade components for ease of reference in subsequent sections of this work. The components of a Venetian blind assembly are depicted in Figure 2.5.

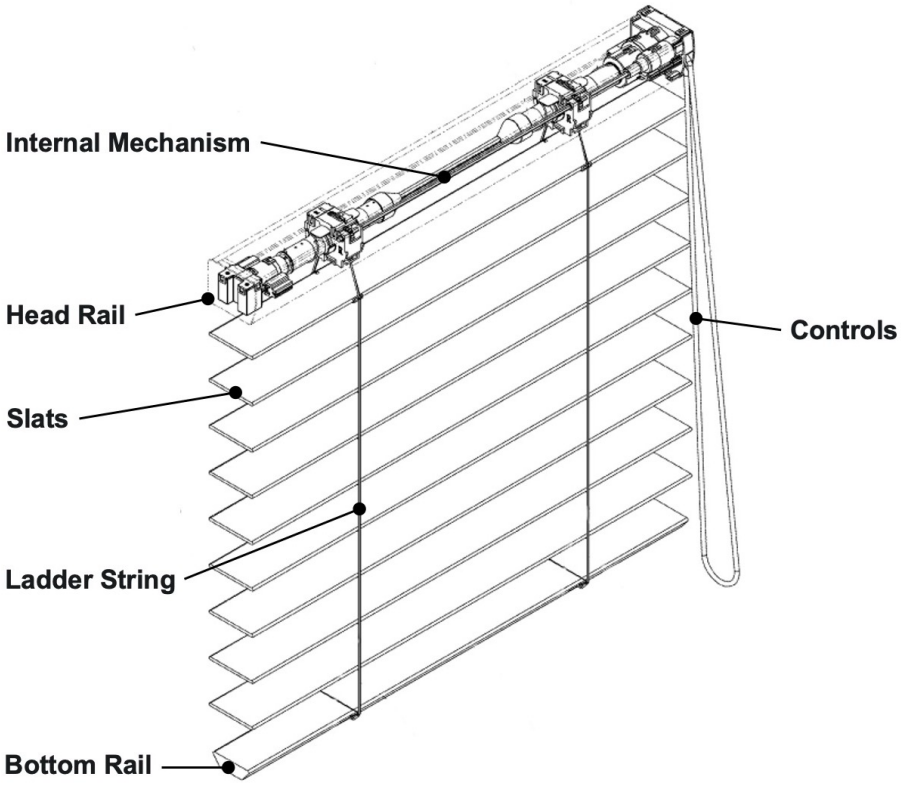

Figure 2.5. Components of a typical window shade assembly (Chen and Nien 2020).

3.0 Survey of Candidate Sensors

In this section, various sensor typologies are introduced, described, and assessed for their relevance regarding blind position sensing. Sensors are grouped based upon sensing technology and the similarity in their implementation approaches. Four broad categories of sensors were examined as part of the initial feasibility screening—time-of-flight sensors, internal rotary encoders, array-based sensors, and exterior linear encoders. All four candidate sensors are characterized in the following sections.

3.1 Time-of-Flight Sensors

The first group of sensors evaluated in this work were time-of-flight sensors. Time-of-flight sensors are characterized by the measurement of time for an object, beam, or wave to collide with an object of interest. This procedure is displayed graphically in Figure 3.1, which shows the sensing technique employed by time-of-flight distance sensors.

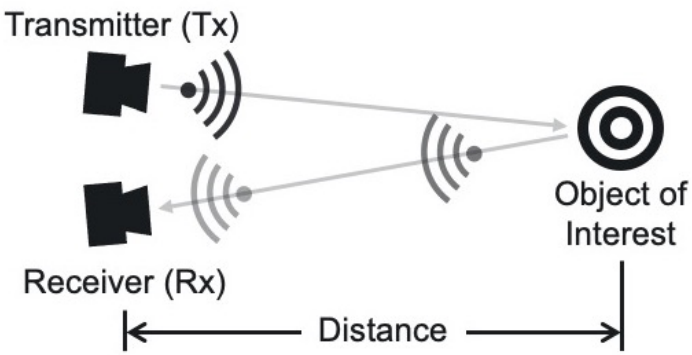

Figure 3.1. Time-of-flight sensor operation.

For most practical time-of-flight applications, mechanical or electromagnetic waves with known velocities are emitted, such as infrared beams or radio waves. In these cases, sensors typically measure the time from emission to absorption of the emitted material to determine the full flight time of the reflected wave. Two typical time-of-flight distance sensor types are infrared time-of-flight sensors and ultrasonic time-of-flight sensors.

One major advantage of time-of-flight sensors for the task of measuring blind displacement is the potential to directly measure absolute blind displacement from the windowsill. For this study, time-of-flight sensors were analyzed in two different configurations: (1) with the sensor affixed to the blind bottom rail, and (2) with the sensor affixed to the windowsill. Both configurations are shown in Figure 3.2.

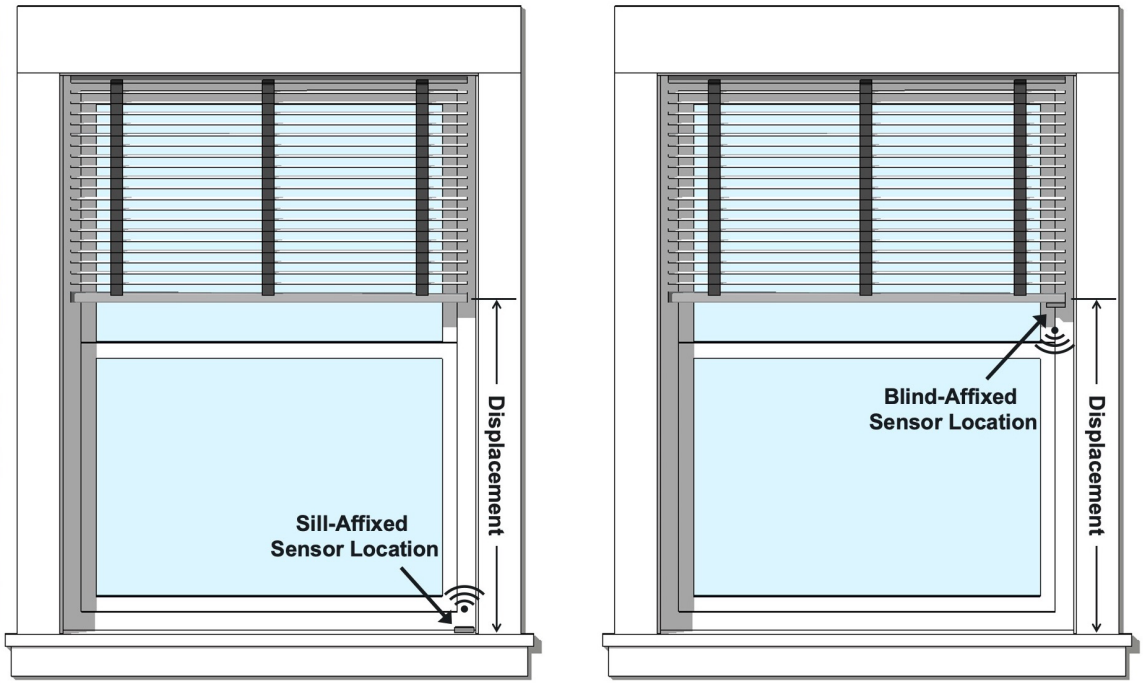

Figure 3.2. Two configurations in which time-of-flight sensors can be oriented to measure blind location.

In theory, these two positions shown in Figure 3.2 should produce similar results; however, sensor type, window geometry, and in-service sensor reliability may differ between the two orientations.

In addition to the two sensor configurations, two different time-of-flight sensors were tested during this study. These sensor types are described in further detail in the following sections.

3.1.1 Infrared Time-of-Flight Sensors

Infrared (IR) time-of-flight sensors are one of the most ubiquitous types of time-of-flight sensors. These sensors emit an IR laser beam, which reflects on the object of interest and is absorbed by the receiver. There are many advantages of these sensors, because the IR beam travels at the speed of light, which can be estimated via environmental conditions.

While IR time-of-flight sensors are ubiquitous, they also have many drawbacks. One major drawback is the potential interference due to reflection and nearby light sources, such as sunlight. It is possible to filter these erroneous frequencies via digital filtering or receiver film coatings, but typical consumer-grade IR distance sensors rarely include these features.

3.1.2 Ultrasonic Time-of-Flight Sensors

Ultrasonic time-of-flight sensors are another popular implementation of time-of-flight sensing. Rather than the laser beams used by IR sensors, these sensors emit ultrasonic sound waves and time these waves' reflection time to the receiver. Because of their application of sound waves, these sensors are fundamentally sonar devices, which can make use of the speed of sound in specific environments, such as in air or water.

Like IR time-of-flight sensors, ultrasonic distance sensors also have drawbacks. Because of the use of ultrasonic frequencies, these sensors are not typically subjected to sonic interference from the surrounding environment; however, ultrasonic distance sensors do suffer from signal spreading. Because ultrasonic time-of-flight sensors emit sound waves from a specially designed speakers these waves broadcast outward from the speaker in a cone-shaped spread. Off-the-shelf ultrasonic distance sensors typically characterize this behavior as an “effectual angle,” which is measured normal to the ultrasonic sensor’s face. This behavior is graphically illustrated in Figure 3.3 to show the influence of the effectual angle.

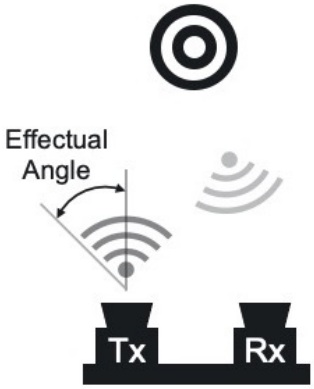

Figure 3.3. Illustration of the effectual angle of ultrasonic time-of-flight sensors.

While the effectual angle makes practical application of ultrasonic distance sensors possible (due to the transmitter and receiver spacing), the effectual angle can also contribute to erroneous readings. In practice, the spread of an ultrasonic sensor’s emission may result in interference from nearby objects. This interference may result in erroneous distance readings, so care must be taken to place the ultrasonic sensor in configurations that reduce interaction with unrelated objects or surfaces.

3.2 Internal Rotary Encoders

The second group of potential sensing candidates is internal sensors—those that connect with or sense the state of the internal mechanism of a shade. Possible implementations of these sensors are encoders attached to pinion rods, blind pull spools, or other mechanisms internal to the operation of a shade. One frequently applied encoder in industrial applications is the rotary encoder. Rotary encoders use mechanical, optical, or magnetic encoding to determine the encoder’s position. Rotary encoder technology can also be subdivided into two major typologies: absolute position sensing and relative position sensing. While less common, absolute position sensing allows for an encoder to determine the position from memory, based upon optical shading, gearing, etc. The most common implementation of rotary encoders is that of a relative position-sensing encoder, which increments measurement via a pre-defined resolution with movement.

While encoders are frequently applied in industrial equipment and robotics to sense position, they have one major flaw when applied to shades—the implementation of shade internal mechanisms varies and causes significant difficulty with the broad application of internal encoders to multiple shade types and brands. Whether shades are corded or cordless, mini-blinds or full-sized, Venetian or roller, there is little consistency in the shade mechanisms or builds, which makes fitting encoders to shade mechanisms a customized implementation for

every shade of interest. Because of these practicality concerns, internal encoding sensors were omitted from testing in this study.

3.3 Array-Based Sensors

Another group of sensors considered for this application is the array-based sensor implementation. This sensor implementation is described as an array of sensors that measure shade position discretely via a collection of sensors arranged in a strip-like configuration. A graphic displaying the array layout of this sensor implementation is shown in Figure 3.4.

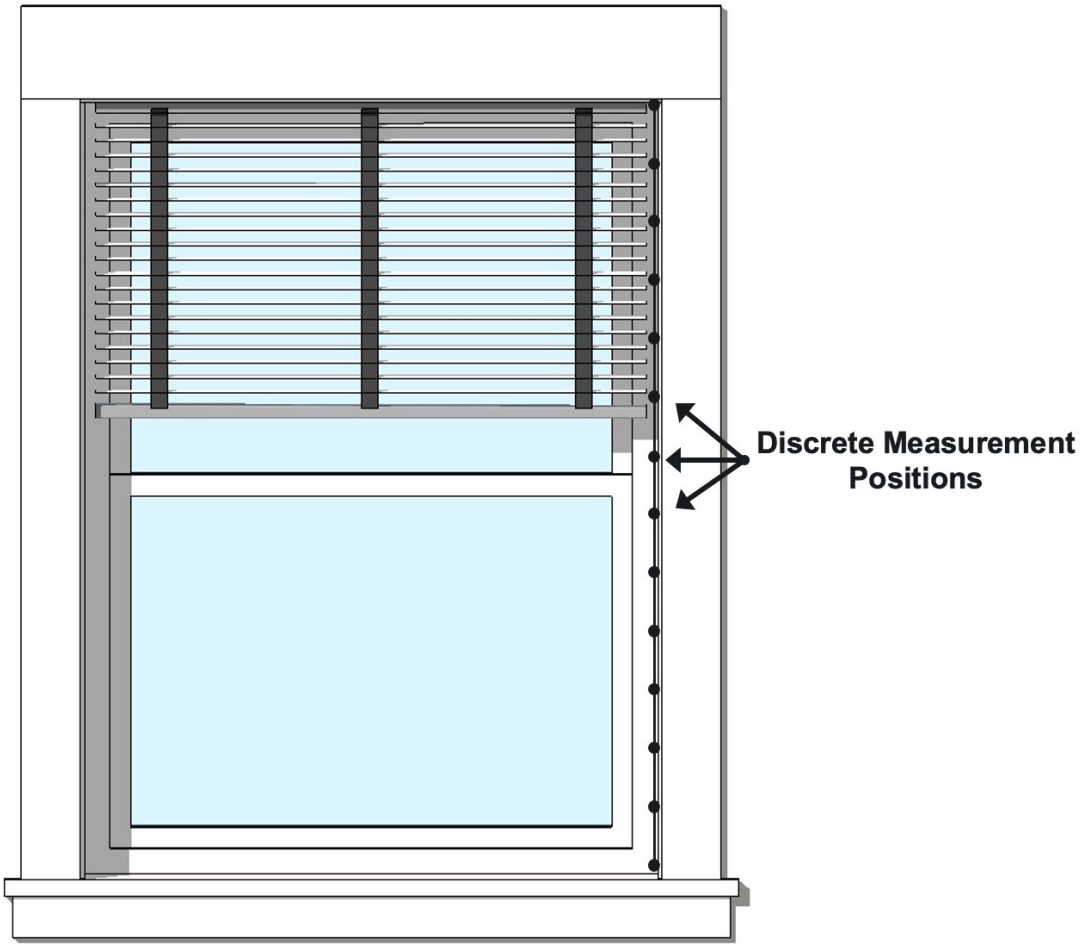

Figure 3.4. Discrete implementation of an array-based shade position sensor.

The concept underlying this sensor implementation is that sensors will report shade position as the shade travels vertically. The resolution of this sensor can be tuned based on the number of implemented sensors, allowing for this sensing approach to be as accurate as required relative to cost and application constraints.

For this sensor configuration, three different discrete sensor types were identified—magnetic reed switches, Hall effect sensors, and photoresistors. Both magnetic reed switches and Hall effect sensors actuate open or closed in the presence of a magnetic field. From an implementation standpoint, reed switches and Hall effect sensors are functionally equivalent. Both sensors actuate between a fully closed or fully open state, depending on the presence or

absence of a magnetic field, which can be introduced via a magnet. The only difference between a reed switch and a Hall effect sensor from a practical standpoint are the internal components—a reed switch is a physical contact that moves as opposed to the fully electrical, solid-state operation of a Hall effect sensor. Because of these minor differences in implementation, Hall effect sensors rather than reed switches were tested in a sensor array.

Photoresistors change resistance in the presence of a light, which may cause complications due to window-specific lighting or indoor lighting fixtures. Because of these potential complications, photoresistors were omitted from testing.

3.4 External Linear Encoders

The final group of candidate sensors identified to measure shade position is linear encoders. Much like rotary encoders, linear encoders are a sensor type heavily used in industrial equipment such as computer-controlled machines and 3D printers. Linear encoders are, as the name suggests, a device that encodes linear position along a fixed axis. In the case of measuring shade height, the fixed axis to which a linear encoder would be affixed is the vertical run of the window side jamb. Affixing the encoder strip to the jamb with the encoder attached to the shade bottom rail would allow for tunable position measurement along the vertical height of the window.

Much like rotary encoders, linear encoders comprise two major categories: absolute position measurement and relative position measurement. Absolute position measurements are made using a specially designed encoder strip, and relative position measurements are made using a standard, uniformly spaced encoder strip. For this application, a few off-the-shelf actual position linear encoders can be readily implemented for the measurement task while also being tall enough for typical window heights. Because of these limitations, an absolute position, magnetic linear encoder strip was sourced for testing and was implemented with a Hall effect sensor to track relative position.

3.5 Summary of the Candidate Sensor Survey

In summary, many sensor candidates were evaluated during the study. Each evaluated sensor comprised unique inner workings, technological concepts, and implementation configurations for measuring shade position. The initial findings and lessons learned from the initial sensor survey are summarized in Table 3.1. Sensors with bolded names were identified as candidates for procurement and testing.

Table 3.1. Summary of sensor survey findings.

Sensor Family	Name	Description
Time-of-Flight	**Ultrasonic Sonar Distance Sensor**	Ultrasonic sound-based time-of-flight distance sensor. Can be attached to the blind or the windowsill.
	Laser Range-Finding Sensor	Infrared laser-based time-of-flight distance sensor. Can be attached to the blind or the windowsill.
Rotary Encoding	Infrared Optical Encoder	External IR motor encoder. Can be attached to blind up/down or rotation shafts to encode location/angle. All internal to the blind mechanism.

Sensor Family	Name	Description
	Potentiometer	Adjustable resistance load. Potentiometer resistance can be correlated to blind angles upon installation.
Array-Based	Photoresistor	Light-sensitive resistor. Can be placed in an array to determine shade position.
	Hall Effect Sensor	Magnetic switching transistor. Can be placed in an array to determine the shade vertical position.
	Magnetic Reed Switch	Magnetic switching relay. Can be placed in an array to determine the shade vertical position.
Linear Encoding	**Magnetic Encoder Strip**	Alternating multi-pole magnetic strip. Can be placed on a window jamb and used with a Hall effect sensor to measure the relative vertical shade location.

From Table 3.1, the sensors that progressed to the testing stage are highlighted. Due to issues with sensor implementation, e.g., sensors not being compatible with certain shade types or logistical hurdles for implementation that could not be solved, the optical encoder, potentiometer, and photoresistor sensing approaches were omitted from testing. The magnetic reed switch was also omitted from testing due to its similarity to the Hall effect sensor. In practice, the reed switch and Hall effect sensor could be used interchangeably, so all findings and recommendations described for the Hall effect sensor could be applied to either approach.

4.0 Experimental Setup and Sensor Implementation

From the initial survey of sensor candidates described in Section 3.0, candidate sensors were selected and sourced for testing. Procurement of candidate sensors prioritized readily available, off-the-shelf sensors and components that could be easily integrated with data acquisition systems. Implementation procedures and required materials varied for each sensor. Implementation specifics are described in detail in subsequent sections.

4.1 Window and Interior Shade for Testing

For the experimental testing, a window with an in-service interior shade was used. Based upon the market characterization presented in Section 2.2, a Venetian blind was selected and installed for testing. A set of white cordless faux wood Venetian blinds was inside-mounted on an east-facing window. This setup allowed for sensors to be installed and monitored during testing. The test window and installed candidate shade are shown in Figure 4.1.

Figure 4.1. Test setup and shade used for sensor testing.

4.2 Data Acquisition System

For this project, a wide variety of sensors were tested in various configurations. Because of the diversity of sensors tested, a robust data acquisition platform was required. For this application, the Arduino MKR Zero was selected as a data acquisition device because of its built-in SD card reader, 15-bit analog-to-digital converter (ADC), and SPI and I^2C serial bus functionality. In addition to having hardware functionality, Arduino MKR Zero is also heavily supported by numerous open-source sensor libraries and sensors designed with platform compatibility in mind. While these benefits were prioritized for the field validation of these sensors, this functionality, along with the low unit cost of an Arduino microcontroller, also makes the Arduino MKR Zero a strong candidate for field deployment.

4.3 Sill-Mounted Ultrasonic Distance Sensor

The first sensor procured and installed on-site was the ultrasonic distance sensor. The ultrasonic distance sensor selected for this project was the HC-SR04 ultrasonic distance sensor. This sensor was selected due to its widespread commercial availability and access to Arduino libraries.

As described in Section 3.1, time-of-flight sensors can be installed in one of two configurations: (1) mounted on the windowsill or (2) mounted on the shade bottom rail. The infrared distance sensor was tested in both configurations in this project. A photograph of the sill-mounted configuration is presented in Figure 4.2.

Figure 4.2. An illustrated photo of the sill-mounted ultrasonic distance sensor tested in this project.

To use the HC-SR04, a few steps were taken to install the sensor. First, the HC-SR04 outputs a 5V signal when measuring distance, which is too high a voltage for the Arduino MKR line. To reduce the voltage of this signal, a voltage divider circuit was built on a breadboard to make this signal compatible with the Arduino MKR Zero. The pre-built SparkFun open-source code for this sensor was deployed with an echo count of two, meaning that the sensor takes two measurements and averages those results to report distance (SparkFun 2020).

After breadboarding and code generation, the HC-SR04 was mounted to a small flat piece of wood trim and secured to the windowsill by double-sided carpet tape. Carpet tape is ideal for the field deployment of windowsill-mounted sensors because of its strong adhesion and easy removability. For all applications in this project, carpet tape left no residue post-removal and did not damage paint.

4.4 Shade-Mounted Ultrasonic Distance Sensor

The second sensor configuration tested was the shade-mounted ultrasonic sensor. As with the sill-mounted ultrasonic sensor, an HC-SR04 ultrasonic sensor was used with an Arduino MKR Zero and was mounted on the bottom surface of the window shade's bottom rail. A photograph of this sensor configuration is presented in Figure 4.3.

Figure 4.3. Shade-mounted ultrasonic sensor configuration tested in this project.

For this test, the HC-SR04 was mounted on the shade's bottom rail with carpet tape and zip ties. This mounting configuration was selected to securely mount the sensor while preventing damage to the shade. Because the sensor was mounted on an operable shade, 15-foot-long ribbon cables were used to connect the sensor to the Arduino MKR Zero for data acquisition. Similar to the sill-mounted ultrasonic distance sensor, this sensor was also deployed using the SparkFun sensor library with an averaging echo count of two (SparkFun 2020).

4.5 Sill-Mounted and Shade-Mounted Infrared Distance Sensors

The second sensor group tested on-site was the infrared time-of-flight distance sensor. The distance sensor selected for this project was the VL53L0X infrared time-of-flight distance sensor. The procured sensor was a VL53L0X sensor attached to a breakout board capable of I^2C communication. Much like its ultrasonic counterpart, this sensor was selected because of its widespread commercial availably, small form-factor, and access to open-source libraries.

Similar to the ultrasonic distance sensor configurations described in Sections 4.3 and 4.4, the infrared distance sensor can be mounted in similar configurations with the same mounting equipment displayed in Figure 4.2 and Figure 4.3, namely 15-foot ribbon cable, zip ties, and double-sided carpet tape. Sensors were connected to an Arduino MKR Zero for data collection

using an open-source Adafruit library for the VL53L0X (Adafruit 2021). Measurements were sampled at a rate of 33 Hz.

4.6 Hall Effect Sensor Array

The fourth sensor configuration tested was the Hall Effect Sensor array. As described in Section 3.3, Hall effect sensors detect the presence of a magnetic field. For this application, a pack of A3144 Hall effect sensors was procured and installed in an array configuration. The sensors were affixed to a 70-inch-long piece of flat wood trim and spaced at 7.75-inch increments. Eight Hall effect sensors were installed in total, allowing for a sensing area of 62 inches (approximately the length of the total shade travel). Figure 4.4 is a photograph of the installed Hall effect sensor array attached to the side jamb.

Figure 4.4. Hall effect sensor array tested in this project.

This array, in combination with a neodymium bar magnet affixed to the end cap of the shade's bottom rail, allows for measurement of the shade's position. In theory, this sensing approach can be tuned to the desired resolution by increasing or decreasing the number of sensors installed in the array. The practical limitation of this approach is the number of channels available on the selected datalogger, because every Hall effect sensor requires its own channel on the logging device. In this implementation, the Arduino MKR unit was programmed using pin interrupts to sense and report changes in voltage associated with certain Hall effect sensors on the array. Not all digital inputs on the Arduino MKR are capable of pin interrupts, so the number of applicable measurement channels was limited to 10 in this application. It should also be noted that the Arduino interrupt service routine operates at a theoretical sampling rate of 9600 Hz, which is reflected as a theoretical polling frequency of 9600 Hz at the Hall effect sensor array.

4.7 Magnetic Encoding Tape

In addition to the array implementation of Hall effect sensors, Hall effect sensors can also be implemented with magnetic encoding tapes to encode the shade position. The final sensing approach tested is composed of an alternating-pole magnetic tape attached to the window side jamb and a Hall effect sensor attached to the end cap of the shade bottom rail. Figure 4.5 is a photograph of the installed encoding strip.

Figure 4.5. The magnetic encoding strip tested in this project.

This tape was installed atop a piece of painter's tape to avoid damage to the window finish. This encoding strip was selected because it could be installed in 3.3-foot increments. The polarity of this encoding strip alternates every 5 mm. For this implementation, two Hall effect sensors were used, known as a leader and a follower, to encode the shade position. This sensor layout and encoding strip relationship is summarized graphically in Figure 4.6, which depicts the use of the leader and follower Hall effect sensors.

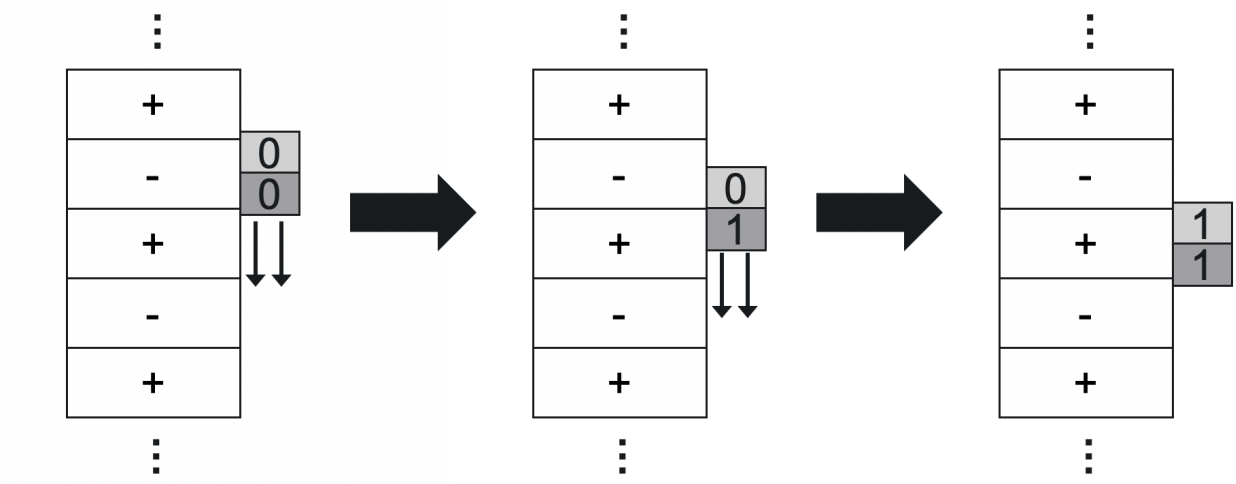

Figure 4.6. Magnetic encoder strip polarity (boxes with polarity) and Hall effect sensor (grey boxes with binary value) operation.

For this example, the leader sensor is the dark grey box and the follower sensor is the light grey box. At the start of the example (on the left), both sensors are reading binary “zeros” due to the local negative encoder pole. As the leader sensor passes the positive encoder pole, the leader sensor reads a binary “one” due to the positive pole, while the follower sensor still reads a “zero” due to its position at the negative pole. As both sensors pass the negative/positive pole interface so that both sensors are experiencing positive polarity, the follower sensor’s value changes to a binary “one,” while the leader maintains the same binary reading. Using an Arduino code with interrupts, these changes in values and their associated pattern can be translated into incremental relative position measurements to determine the sensor, and by association, the shade position along the run of the magnetic encoding strip. Note that this sensing approach is only valid if the Hall effect sensors are within sensing distance of the encoding strip’s magnetic field.

4.8 Implementation Summary

In conclusion, four sensing approaches were installed in six sensing configurations for testing. Table 4.1 lists the estimated implementation costs of each sensing approach, excluding the cost of the Arduino unit used for data acquisition. More detailed material cost breakdowns for each sensing approach can be found in Appendix A.

Table 4.1. A tabulated summary of the sensor approaches and costs for each sensor implementation tested in this study.

Sensor Type	Sensor Model	Raw Material Cost ($)	Implementation Effort (Qualitative Assessment)
Sill-Mounted Ultrasonic Distance Sensor	HC-SR04	$6.75	Low

Sensor Type	Sensor Model	Raw Material Cost ($)	Implementation Effort (Qualitative Assessment)
Shade-Mounted Ultrasonic Distance Sensor	HC-SR04	$7.06	Medium
Sill-Mounted Infrared Distance Sensor	VL53L0X	$11.75	Low
Shade-Mounted Infrared Distance Sensor	VL53L0X	12.06	Medium
Hall Effect Sensor Array	A3144	$18.78	High
Magnetic Encoder Strip	A3144/Adafruit #4680	$101.55	High

5.0 Experimental Design and Results

To evaluate sensor performance, feasibility, and reliability, a field experiment was designed to simulate typical in-service conditions that each sensor could be expected to undergo. Each of the proposed sensor technologies was installed on an operable Venetian shade. Two tests were conducted on each of the candidate sensors outlined in Section 4.0. Testing was conducted over seven days spread across two months. The candidate blind used was a faux wood Venetian blind installed in an inside-mount orientation on an east-facing window.

5.1 Newly Installed Sensor Accuracy

The blind's vertical position was raised and lowered manually to prescribed positions, manually measured using a tape measure, and measured by each of the proposed position-sensing technologies. The prescribed shade positions were spaced every 6 inches along the vertical travel of the blind, which is approximately 60 inches long. Position and state measurements made by the proposed sensor technologies were then compared to the manual measurements to determine the accuracy of each of the sensor technologies. Because of the inherent variability in sensor readings among time-of-flight sensors, each reading taken by an ultrasonic or infrared distance sensor was repeated for 1000 samples to capture sensor uncertainty.

5.2 Simulated "In-Service" Sensor Reliability

In addition to exhibiting sensor accuracy, sensor reliability and repeatability are equally important when assessing sensor feasibility for field studies. To capture the variability between newly installed sensors and sensors that have been in service for some time, i.e., simulating performance in a field study, a second set of tests was conducted. For these tests, each sensor was installed on a set of Venetian blinds that were raised and lowered 10 times over 24 hours. After this waiting period, the procedure described in Section 5.1 was followed. This test was designed to capture issues related to physical agitation and offset error, which may occur during sensor service at a field site.

5.3 Sill-Mounted Infrared Distance Sensor Results

The first sensor tested was the infrared distance sensor attached to the windowsill via double-sided carpet tape. The sensor was placed near an inside corner of the window, at the interface of the window sash and side jamb. Results from testing this sensor are shown in the box plot and histogram presented in Figure 5.1.

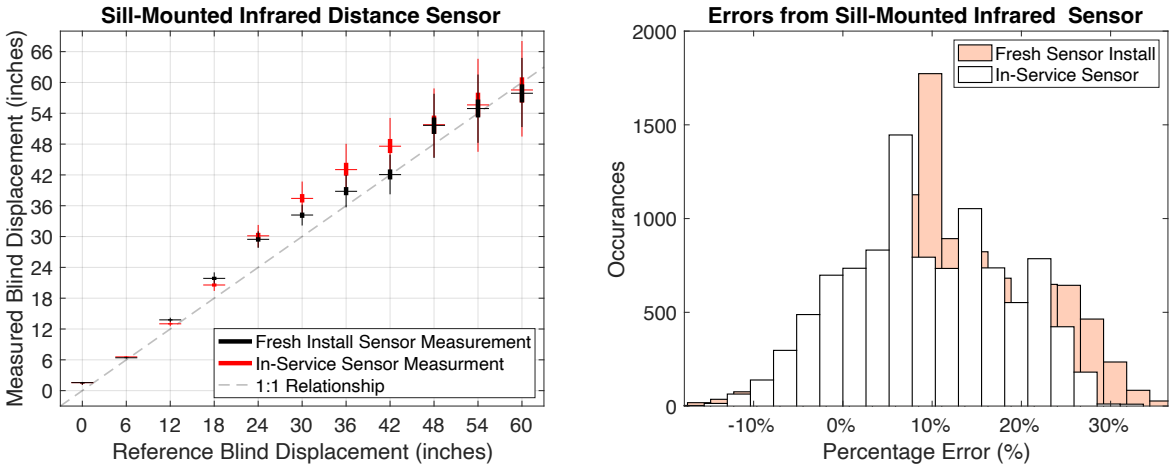

(a) Sensor Accuracy Evaluation Boxplot (b) Sensor Absolute Error Histogram

Figure 5.1. Testing outcomes for the windowsill-mounted infrared time-of-flight sensor.

The boxplot displays the stochastic performance of the sensor at the various test points, both post-install and after 24 hours of operation. The percentage error was also computed for all non-zero reference measurements for both tests and is displayed in the histogram. From these tests, it was noted that the average error for the post-installation sill-mounted infrared distance sensor was 9.33% and 14.0% after 24 hours of being in service. It was also noted that sensor measurements began to diverge from reference measurements near a blind displacement of 18 inches, then reconverged upon the reference measurements near a displacement of 54 inches. Measurement standard deviations also increased as the shade displacement increased. The occurrence of these phenomena in both tests is believed to be a result of sunlight interacting with the infrared beam, most likely related to the blind and window frame shading near the bottom and top of the blind travel.

5.4 Shade-Mounted Infrared Distance Sensor Results

The second sensor configuration tested was the infrared distance sensor attached to the shade's bottom rail via zip ties. The sensor was centrally located on the shade's bottom rail, aimed directly at the windowsill. The stochastic results of this testing are shown in the box plot and histogram presented in Figure 5.2.

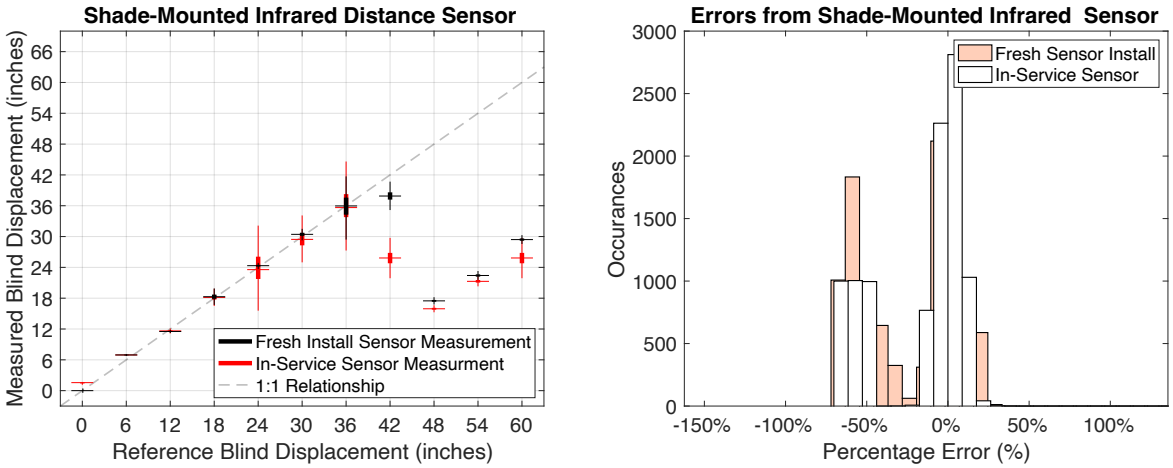

(a) Sensor Accuracy Evaluation Boxplot (b) Sensor Absolute Error Histogram

Figure 5.2. Testing outcomes for the shade-mounted infrared time-of-flight sensor.

In Figure 5.2b, the bimodal nature of the sensor error is immediately apparent, indicating an underlying phenomenon captured through both rounds of testing. This phenomenon is also present in the accuracy boxplot—the sensor remained relatively accurate for blind displacements up to 36 inches, then measurements rapidly diverged from reference values as displacement increased. It was noted during testing that the shade bottom rail did not remain paraellel to horizontal sill due to the location of the shade lift cord connection point. Because the lift cords were connected at one point on each side of the shade (as opposed to the two connection points present for the tilting cords), the Venetian blind bottom rails appeared to be a neutrally unstable system that naturally tended to tilt toward or away from the window when at rest. This tilting phenomenon explains the low measured displacement values displayed in Figure 5.2a at reference measurements of 42, 48, 54, and 60 inches; it appears that the blind tilted toward the window, pointing the distance sensor at the window rather than at the windowsill. Because of these issues, mean error values of 46.6% and 99.9% were computed for this sensing approach.

5.5 Sill-Mounted Ultrasonic Distance Sensor Results

The third sensor configuration tested was the ultrasonic distance sensor attached to the windowsill via double-sided carpet tape. This sensor was leveled using a bubble level to guarantee that the sensor was aimed at the shade. Much like the sill-mounted infrared distance sensor tested in Section 5.3, this sensor was installed at the interface of the window sash and side jamb. The results of this test showing the performance of the sill-mounted ultrasonic distance sensor are shown in the boxplot and histogram presented in Figure 5.3.

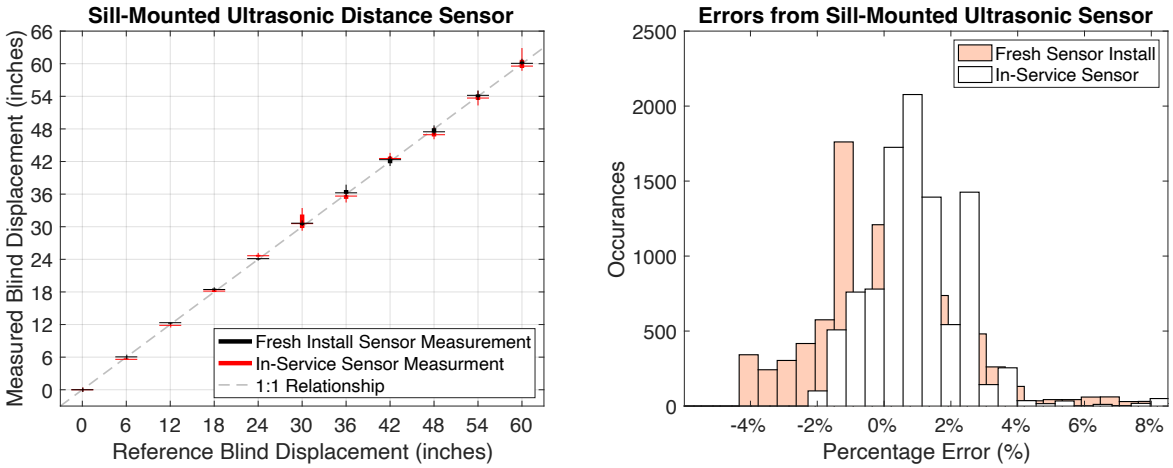

(a) Sensor Accuracy Evaluation Boxplot (b) Sensor Absolute Error Histogram

Figure 5.3. Testing outcomes for the windowsill-mounted ultrasonic time-of-flight sensor.

From these results, it was noted that this sensor configuration produced more accurate results than the two previously tested configurations, with mean errors of 1.26% and 1.93% for post-installation performance and performance after 24 hours of being in service. No major diversions from reference measurements were observed with this sensor, indicating little disturbance by environmental factors. Sensor repeatability differed slightly between the two tests—measurement standard deviation was 3.62% error post-install and 19.2% after 24 hours of being in service. This difference in error standard deviation for the latter test appeared to be driven by large standard deviations at the 30- and 60-inch reference measurements. It was noted that the window's top rail was near the 30-inch reference point, possibly contributing to the variation in measurement at that location.

5.6 Shade-Mounted Ultrasonic Distance Sensor Results

The fourth sensor configuration tested was the ultrasonic distance sensor attached to the shade's bottom rail via zip ties. The results of this testing, showing the performance of the shade-mounted ultrasonic distance sensor are shown in the boxplot and histogram presented in Figure 5.4.

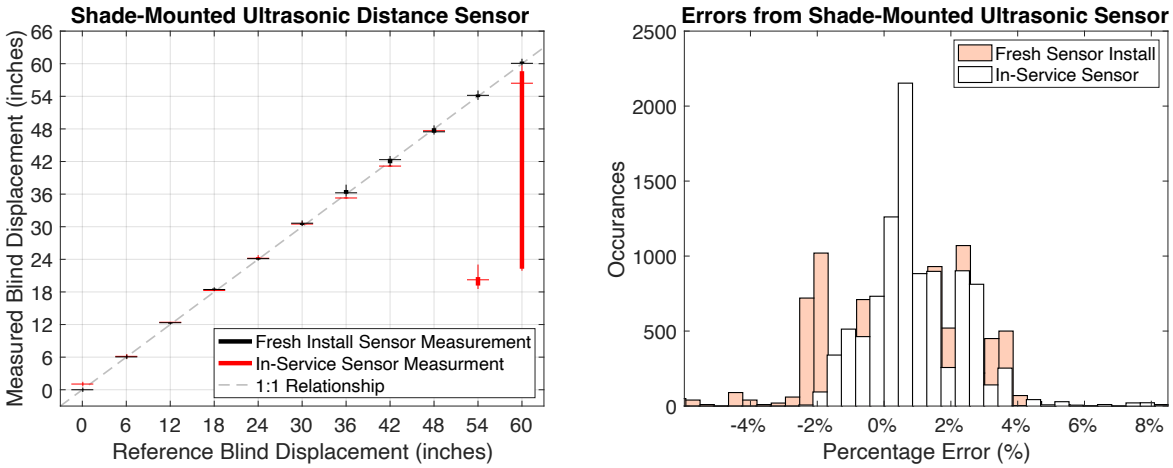

(a) Sensor Accuracy Evaluation Boxplot (b) Sensor Absolute Error Histogram

Figure 5.4. Testing outcomes for the shade-mounted ultrasonic time-of-flight sensor.

From these results, it was noted that this sensor configuration produced more accurate results than the shade-mounted infrared distance sensor, with means errors of 4.26% and 21.1% for both tests, respectively. Despite the improved accuracy relative to the other shade-mounted sensor, the shade-mounted ultrasonic distance sensor also displayed similar issues related to shade bottom rail tilting, as indicated by measurements made at reference displacements of 54 and 60 inches.

5.7 Hall Effect Sensor Array Results

The fifth sensor configuration tested was the array of Hall effect sensors arranged in a strip pattern. As stated in Section 4.6, these sensors were attached to a thin length of wood and connected to multiple digital channels of an Arduino MKR Zero. This sensor configuration's performance is summarized in a scatterplot in Figure 5.5.

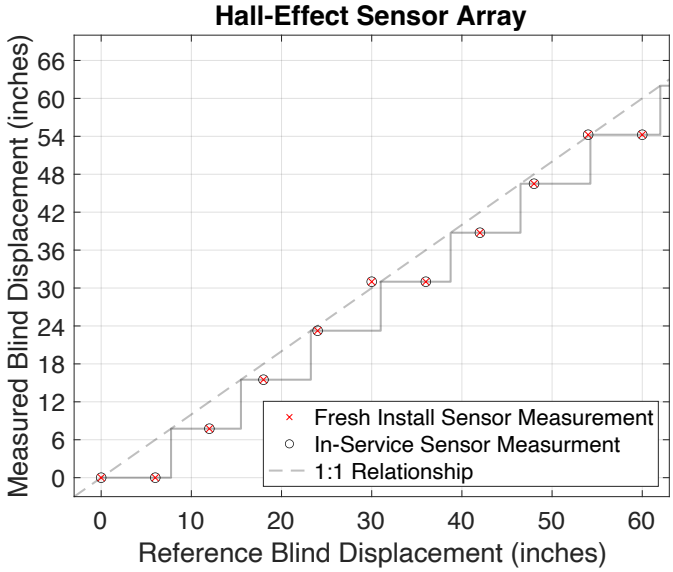

Figure 5.5. Accuracy results for the jamb-mounted array of Hall effect sensors.

It should be noted that this sensor's output does not lend itself to a boxplot or histogram presentation. Unlike the time-of-flight sensors tested, this sensing approach does not report a distance, it reports the position of the last Hall effect sensor triggered by the blind's movement. As a result of this functionality, the resolution of this sensing approach is as accurate as the resolution of the sensor array, which in turn is limited by the number of available interrupt-enabled channels on the data acquisition system. In this case, the Arduino MKR Zero had eight interrupt-enabled channels, allowing for a resolution of 7.75 inches along the 60-inch blind travel.

Through both rounds of testing, this sensor configuration was calculated to have a percentage error of 18.3%. Despite the Hall effect sensor array's accuracy placing it in the lower quartile of sensors tested, this sensing approach is quite powerful because of its reliability. Both the freshly installed sensor array and sensor array tested after 24 hours of operation produced the same results. The repeatability of this approach makes this sensing approach an attractive candidate for energy efficiency studies where tenths or quartiles of the shade travel may be more than enough information.

5.8 Magnetic Encoding Tape Results

The final sensor configuration tested was the set of two Hall effect sensors used with a multi-pole magnetic encoding tape. The results of this testing group are displayed the scatterplot presented in Figure 5.6.

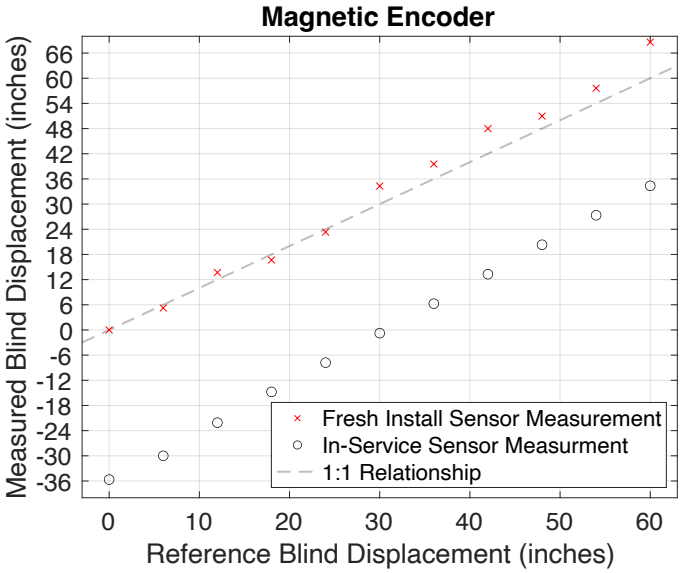

Figure 5.6. Accuracy results for the jamb-mounted magnetic encoder strip.

From these results, it is apparent that the post-installation performance of this approach differs drastically from performance of this sensing approach after a short time of being in service. Computed percentage mean percentage error values are 5.70% and 160% for the post-installation sensor test and sensor after 24 hours of being in service. Based upon the poor performance of this sensor after 24 hours of being in service, it is was concluded that this error is a result of compounding error, which may occur because the Hall effect sensors are not interfacing with the encoding strip during blind travel. If present, these interfacing errors would compound, causing the approach to become less accurate over time. One possible solution to

address this issue would be to either (1) use an absolute position encoder and encoder strip (most likely repurposed from an industrial application) or (2) reset the sensor position measurement at various points along the blind travel. Regardless, neither of these solutions is simple to implement or an “off-the-shelf” solution, which places potential fixes outside the scope of this project.

6.0 Learnings from Survey and Testing

In this study, six sensing approaches were tested in two different trials to evaluate shade position. Ultrasonic time-of-flight sensors, infrared time-of-flight sensors, Hall effect sensors, and a magnetic linear encoder tape were tested, with the time-of-flight sensors installed in two different orientations. Testing was conducted on newly installed sensors and sensors that had been deployed for 24 hours with a shade that was raised and lowered 10 times. Through the experience of installing, operating, and testing each sensing approach, many lessons were learned.

The first major observation from this exercise was that there are inherent problems with installing sensors directly onto a shade. The performance of both the shade-mounted sensors (the shade-mounted infrared distance sensor and the shade-mounted ultrasonic distance sensor) degraded after 24 hours of being in service. The shade-mounted infrared distance sensor, which had poor performance on both tests, degraded in accuracy from 46.6% to 99.9% after a short time of being in service, and the shade-mounted ultrasonic distance sensor degraded in accuracy from 4.26% to 21.1% after 24 hours of being in service. The poor performance of both of these sensing approaches can be attributed to the sensor mounting style because the bottom rail of Venetian blinds does not always remain level with the windowsill. In addition to accuracy issues, attaching sensors to the shade itself requires the sensors to be wired to a data acquisition platform, resulting in unsightly wires hanging from the shade assembly. These wires must be long enough to account for the full travel of the shade and they require strain relief, allowing for an additional failure point of the sensing approach. Because of these limitations, it is not recommended that sensors be attached to a shade's bottom rail, or on the shade itself.

Another notable observation from testing was the performance gap between infrared distance sensors and ultrasonic distance sensors when attached to the windowsill. Ultrasonic distance sensors outperformed infrared distance sensors with an accuracy of 1.26% error post-install and 1.93% compared to the infrared distance sensor's mean accuracy of 9.33% and 14.0% for the two trials, respectively. Sill-mounted ultrasonic distance sensors also outperformed sill-mounted infrared distance sensors from a repeatability perspective—ultrasonic sensors had a standard deviation of error of 3.62% and 19.2% for each trial respectively, while sill-mounted infrared distance sensors had a standard deviation of error of 9.03% and 21.7% for each trial, respectively. These performance increases were likely a result of environmental factors affecting the infrared sensor, and the ultrasonic sensor's effectual angle. Because of the slight spread of the ultrasonic sensor's emitted soundwave, it was noted that the sensor would still operate even if it was not oriented exactly at the shade. The beam emitted by infrared sensors only travels in a straight line, so any slight misalignments with the sensor and sensing surface can result in erroneous readings. For use in the field, the ultrasonic distance sensor mounted on a windowsill appears to be a more robust, reliable, and repeatable option than the infrared distance sensor.

The other two sensing approaches tested were based upon Hall effect sensors and magnets (Hall effect sensor array and magnetic encoding approaches). Briefly, the magnetic encoding tape and Hall effect sensor combination produced strong results with an average percent error of 5.70%, but this accuracy quickly degraded to a 160% mean error due to compounding error. Considering that this sensing approach was the most expensive from a materials perspective and can potentially encounter issues with compounding error, this sensing approach is not recommended for field deployment. Despite the poor performance of the encoding strip, the

vertical array of Hall effect sensors performed well with a mean error of 18.3%. While this mean error is not a low value compared to those of the other sensors tested in this study, it should be noted that this sensor produced the same result both after deployment and after 24 hours of being in service. This sensor produced the same outputs on each of the 10 times the shade was modulated. This repeatability makes the array of Hall effect sensors a strong candidate for field deployment in energy efficiency studies. The mean error displayed in this study is a result of the array's eight-sensor composition; the accuracy and resolution of this approach can be drastically increased by increasing the number of sensors installed in the array. This study was limited by the number of available interrupt channels on the data acquisition system; however, this problem can be readily addressed via data acquisition platform selection.

7.0 Recommendations for Field Deployment

Based on the survey and experimental testing, three window attachment sensing strategies were identified as effective options for field deployment:

- Windowsill-mounted ultrasonic distance sensor
- Windowsill-mounted infrared distance sensor
- Array of Hall effect sensors

While all three sensing approaches provide repeatable results, each sensor has strengths and weaknesses that make it better suited for certain applications. Both distance sensors have similar applicability, implementation, and underlying principles, but the ultrasonic sensor outperformed the infrared sensor in this study. Despite this, there are still some applications where the infrared sensor may be preferable. Notes on the practical implementation of these sensors are outlined in more detail in the following sections.

7.1 Integration with Venetian Blinds

From the market characterization study presented in Section 2.2, it was concluded that horizontal Venetian shades were the most prominent shade type in American homes. For this reason, all testing presented in this study was conducted on a Venetian shade so all implementation information presented in Section 4.0 can be followed for application with Venetian blinds. Regardless, both the ultrasonic distance sensor and Hall effect sensor array approaches can be applied to Venetian blinds, whether they are mini-blinds, wood, faux wood, or vinyl. Given the thickness of Venetian blinds, the ultrasonic distance sensor may be the best candidate for this application from the perspective of measurement accuracy. When applying this sensor with Venetian blinds, it is recommended that the ultrasonic distance sensor be mounted in the bottom corner of the window frame, at the interface with the windowsill, sash, and side jamb. This recommended placement is depicted in Figure 7.1.

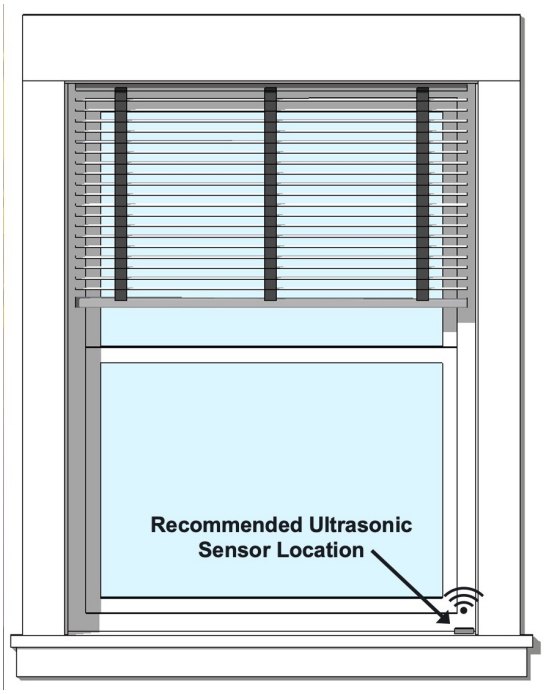

Figure 7.1. The recommended mounting location of an ultrasonic distance sensor for shade position measurement.

Based on preliminary testing and troubleshooting during this project, this location appeared to produce the most reliable results because of the lack of protruding geometry, which may cause interference with measurement. Care must still be taken to align the sensor with the shade bottom rail, but the effective angle and reflection make ultrasonic distance sensors slightly more "forgiving" than infrared distance sensors in this orientation.

7.2 Integration with Vertical Blinds

The second most prevalent blind type found in the market characterization study was vertical blinds. Given the unique orientation of vertical blinds, special considerations must be accounted for when installing a sensor to sense the position of these blinds. The first major consideration is the length of blind travel—vertical blinds tend to have a significantly longer travel than traditional Venetian shades. The HC-SR04 used in this study is reported to have a maximum ranging distance of 9.84 feet, so it is not recommended to use this sensor on blind travels greater than the recommended ranging distance. If shade travel is greater than 9.84 feet, then a long-range infrared distance sensor may be better suited for the application. Regardless of the specification of the time-of-flight sensor, it is recommended that the sensor be installed so that the wave or beam emitted travels parallel to the vertical shade's track and is aimed at the shade's louver.

The second major consideration with sensing vertical blind position is the fore-aft movement of the blinds during operation. This movement is a result of the louvers being fixed at one point rather than two points, causing louver sway during blind actuation. This sway may cause issues when integrating a Hall effect sensor array with vertical blinds, so it is recommended that time-of-flight sensors be the only position sensors used with vertical blinds.

7.3 Integration with Roller Shades

Another popular shade type is roller shades. While roller shades only make up 4% of the residential window attachment market share, roller shades are a popular window attachment type in commercial buildings. One of the major considerations when deploying sensors for roller shades is the thickness of the shade's bottom rail. Roller shades tend to comprise of a heavy fabric with a thin bottom rail. As a result, time-of-flight sensors may have difficulty sensing the bottom rail's location; therefore, it is recommended that a Hall effect sensor array be deployed on roller shades, along with other shades with thin bottom rails such as Roman shades, also known as pleated shades. It is recommended that the Hall effect sensor array be installed along the window's side jamb, as shown in Figure 4.4. The permanent magnet should be affixed to the shade bottom rail's end cap with a sturdy tape or adhesive.

7.4 Integration with Other Blind Styles

For all other blind styles, learnings from this study can generally be applied to the use of other shade types. For shade types not covered in this section, it is recommended that users identify the shade types closest to their shade of interest and apply those recommendations. For example, cellular shades tend to have bottom rails that are approximately the thickness of a Venetian blind. Because of this thickness, it would be wise to follow the recommendations for integration with Venetian blinds. Another example for consideration is integration with Roman shades. Roman shades tend to be fabric with a thin bottom rail, so referring to the section about integration with roller shades for integration suggestions is recommended.

7.5 Integration with Data Acquisition Platforms

While this study used the Arduino MKR Zero as a data acquisition platform, sensor implementation and measurement with another platform may be required for a specific project. To provide context for the integration of the ultrasonic distance sensor and Hall effect sensor array, this section provides schematics and pseudo-code for sensor implementation with Arduino and a Campbell Scientific Datalogger. The Campbell Scientific CR-1000 is used as an example industrial datalogger. Additional information may be required for implementation with other platforms, but the wiring diagrams and pseudo-code should be like that of the CR-1000.

7.5.1 Ultrasonic Sensor Implementation with Arduino

The ultrasonic distance sensor used in this study was the HC-SR04. This sensor is an off-the-shelf distance sensor that is widely used in the Arduino community. As stated in Section 4.3, the open-source Sparkfun Arduino library was used to operate the sensor, but numerous other open-source HC-SR04 Arduino libraries are published on GitHub.

In addition to the code, a proper wiring setup is required for sensor operation. An example wiring diagram for connecting the HC-SR04 to the Arduino is shown in Figure 7.2.

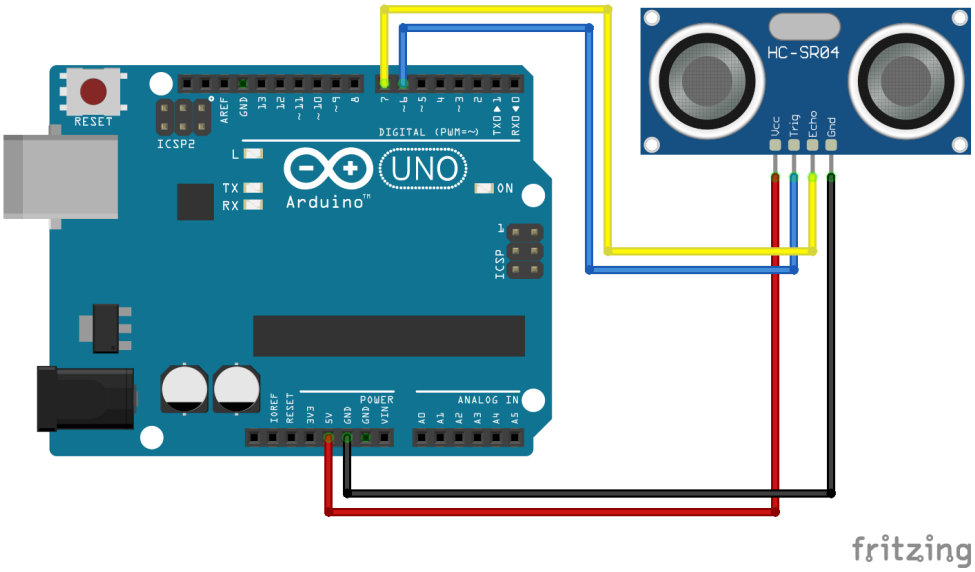

Figure 7.2. A sample HC-SR04 wiring diagram for an Arduino.

The wiring is fairly straightforward—the 5V pin on the Arduino is connected to the power pin on the sensor, the ground pin on the Arduino is connected to the ground pin on the sensor, and the sensor's trigger and echo pins are connected to digital pins on the Arduino. It is important to take note of the pin numbers connected to the digital and echo pins because they will be declared in the Arduino code.

7.5.2 Ultrasonic Sensor Implementation with Campbell Scientific CR1000

While the two systems are visually very different, ultrasonic distance sensor implementation for the Campbell Scientific CR1000 does not differ drastically from that of an Arduino. Power pins on the CR1000 are connected to power channels on the HC-SR04 and digital channels on the CR1000 are connected to the sensor's trigger and echo pins. A CR1000 wiring schematic for the HC-SR04 is shown in Figure 7.3,

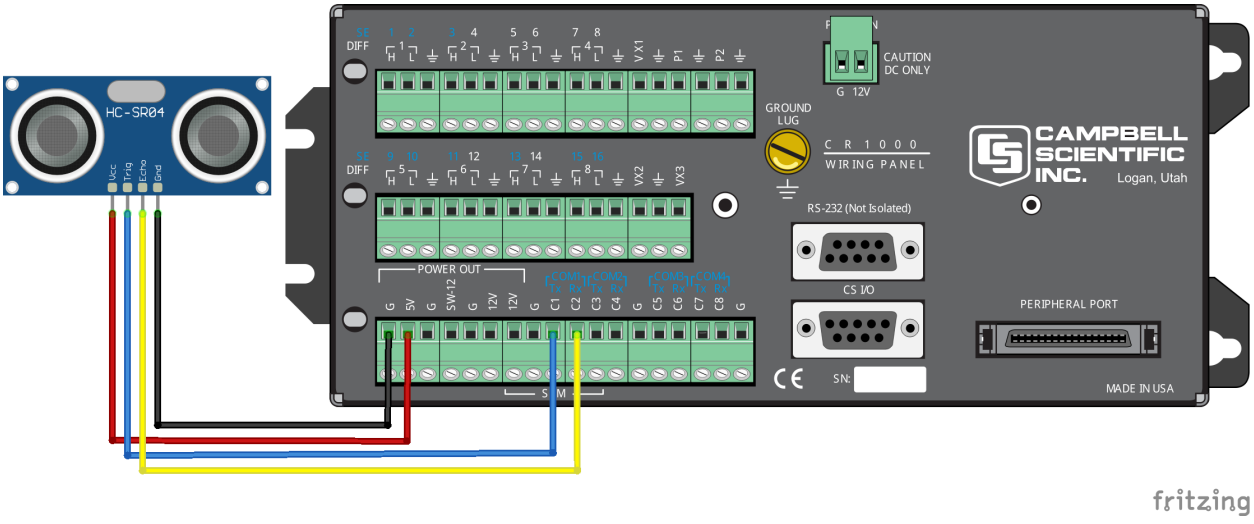

Figure 7.3. A sample HC-SR04 wiring diagram for the Campbell Scientific CR1000 datalogger.

While it is important to correctly wire the sensor to the data acquisition system, the major hurdle in sensor implementation is writing code for the specific platform. In this case, it appears that the CR-1000 does not have any support for the HC-SR04 distance sensor, so code would have to be adapted for the platform. For reference, a portion of the pseudo-code for this approach is presented in Appendix B of this document.

7.5.3 Hall Effect Sensor Array Implementation with Arduino

The Hall effect sensor used in the Hall effect sensor array is the A3144. This sensor is a generic Hall effect sensor that can be operated at voltages ranging from 2.5 V to 5 V. As stated in Section 4.6, the Hall effect sensors were attached to a piece of wood and were wired to the Arduino. In this study, eight Hall effect sensors were arranged in a vertical array orientation. As an example, a wiring diagram for three A3144 Hall effect sensors wired to an Arduino is shown in Figure 7.4. Note that this example uses an Arduino MKR rather than an Arduino Uno. Hall effect sensor operation requires the use of interrupt-enabled pins, and the Arduino Uno only has two interrupt pins while the Arduino MKR series has 10 interrupt pins at pins 0, 1, 4, 5, 6, 7, 8, 9, A1, and A2.

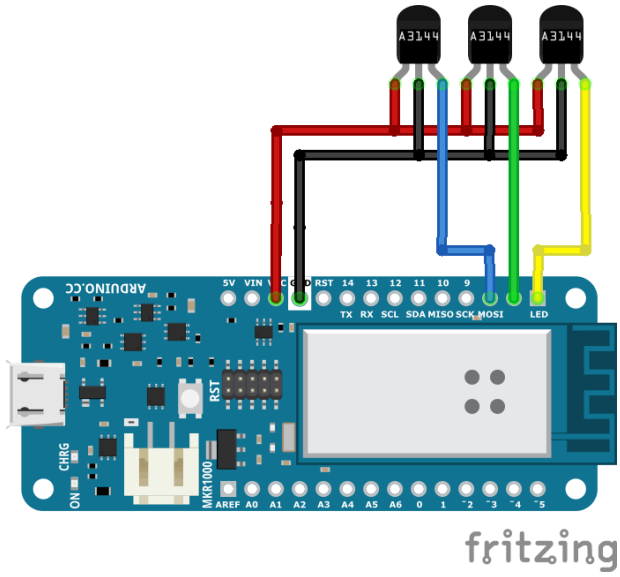

Figure 7.4. A sample Hall effect sensor array wiring diagram for an Arduino MKR series microcontroller.

As stated previously, sensor code is as important as sensor wiring for data acquisition. Because the Hall effect sensor array is a custom sensor implementation, custom code was written in favor of using code from an open-source library. Pseudo-code for this approach is presented in Appendix C.

7.5.4 Hall Effect Sensor Array Implementation with Campbell Scientific CR1000

Hall effect sensor implementation with the CR1000 is very similar to that of an Arduino. The 5V connections are bridged, ground connections are bridged, and digital channels are connected to the output legs of each Hall effect sensor. One major difference between the CR1000 and an Arduino MKR is the location of digital interrupt pins. An Arduino MKR series board has 15 digital pins and 10 interrupt-enabled pins. Not every digital pin on an Arduino has access to the interrupt service routine. A CR1000 has 8 digital pins and 8 interrupt pins, labeled C1–C8. All

digital pins on a CR1000 have access to the interrupt service routine. A wiring schematic for the Hall effect sensor array implementation on the Campbell Scientific CR1000 is shown in Figure 7.5. Pseudo-code for this approach can also be found in Appendix C.

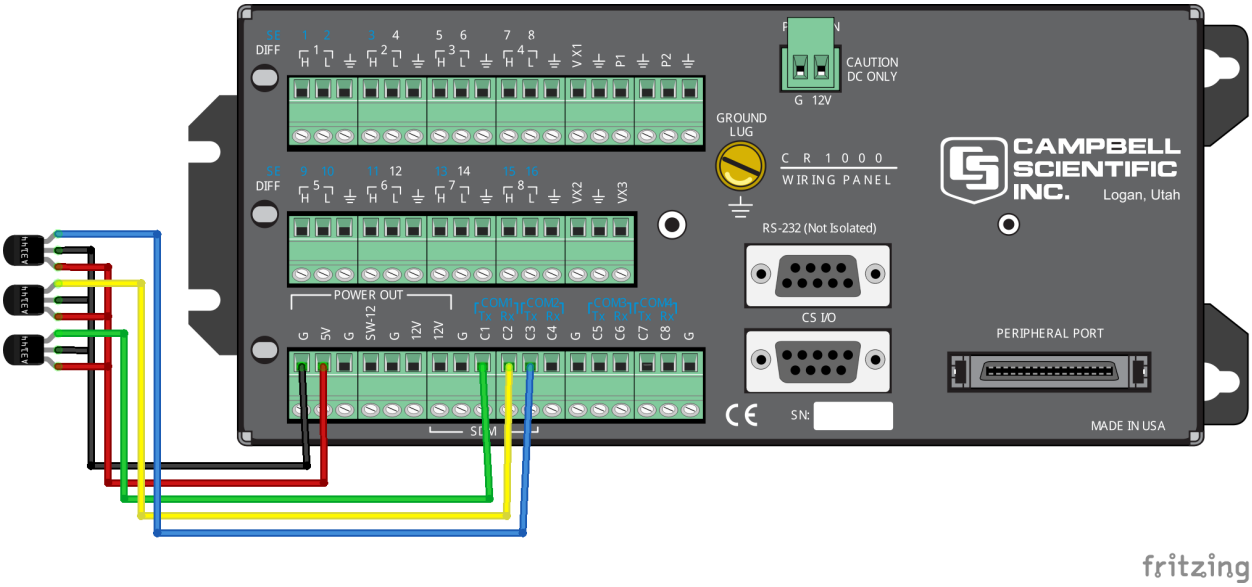

Figure 7.5. A sample Hall effect sensor array wiring diagram for the Campbell Scientific CR1000.

8.0 Conclusion

In conclusion, windows are a major source of energy loss in buildings. To combat these thermal losses, window attachments, such as shades or blinds, can be deployed to lessen the amount of heat gain or heat loss occurring through windows. From an energy efficiency perspective, a major drawback of operable window attachments is their uncertainty of operation. This problem can be somewhat mitigated by installing automated shades, which are slowly gaining a market share; however, users can also overwrite schedules, reintroducing a factor of uncertainty in the energy impact of window attachments.

To address the uncertainty in shade usage and performance, this study was undertaken to identify capable options for sensing shade position accurately and reliably for field-based studies. This study surveyed the current state of the window attachments market; identified candidate sensors to measure shade position; procured, installed, and tested these sensors; and identified two candidate sensors for application in window blind-related energy efficiency studies. It was found that 44% of the residential window attachments market comprises horizontal Venetian blinds. Eight potential sensor types were identified and were pared down to four types of procured sensors that could be implemented in six unique configurations. Each of these six sensing approaches was tested on an installed Venetian blind. Two rounds of testing were conducted, comparing the sensor output to a reference measurement as the blind traveled vertically up the window. Testing was split into two discrete tests—the first test occurred immediately after sensor installation, and the second test occurred after the sensor had been in service for 24 hours and the blinds had been actuated open and closed 10 times. The six sensing approaches tested were:

- an ultrasonic distance sensor mounted to the windowsill,
- an ultrasonic distance sensor mounted to the shade,
- an infrared distance sensor mounted to the windowsill,
- an infrared distance sensor mounted to the shade,
- an array of Hall effect sensors, and
- a magnet-based linear encoding approach.

Of the approaches tested, the three sensing approaches that exhibited the best performance were the windowsill-mounted ultrasonic distance sensor, the windowsill-mounted infrared distance sensor, and the array of Hall effect sensors. Because of the similarities in application between the ultrasonic and infrared distance sensors, the ultrasonic distance sensor should take priority over the two sensors due to its superior performance in this study (1.60% average error between the two tests compared to the 11.7% average error for the infrared sensor). Another important aspect of these selected sensors is their price—all three of the top-performing sensors had a material cost below $20 per window, while the two distance sensors had a material cost under $12 for deployment per window.

This study is a foundational step toward acquiring further understanding of the energy performance of window attachments. The sensors identified by this project provide the opportunity to quantify occupant interaction with their window attachments reliably and accurately at a low cost. In the future, these findings will ideally be deployed in a field study to quantify shade operation and identify much-needed representative operating schedules to accurately represent window attachment use.

9.0 References

Adafruit. (2021). *Adafruit VL53L0X Library*. https://github.com/adafruit/Adafruit_VL53L0X

Bavaresco, M. V, & Ghisi, E. (2018). Influence of user interaction with internal blinds on the energy efficiency of office buildings. *Energy and Buildings*, *166*, 538–549.

Bickel S, E Phan-Gruber, and S Christie. 2013. *Residential Windows and Window Coverings: A Detailed View of the Installed Base and User Behavior.* Prepared for the U.S. Department of Energy's Office of Energy Efficiency and Renewable Energy. September 2013. D&R International, Silver Spring, Maryland. Available online at: https://www.energy.gov/sites/prod/files/2013/11/f5/residential_windows_coverings.pdf

Chen, L., & Nien, K.-H. (2020). *Window Blind* (Patent No. US 10,619,410 B2). United States Patent Office. https://patentimages.storage.googleapis.com/6a/13/10/c718283a863070/US10619410.pdf

Cort, KA, JA McIntosh, GP Sullivan, TA Ashley, CE Metzger, and N Fernandez (2018). "Testing the Performance and Dynamic Control of Energy-Efficient Cellular Shades in the PNNL Lab Homes. PNNL-27663 Rev 1. Pacific Northwest National Laboratory. August 2018.

Curcija DC, M Yazdanian, C Kohler, R Hart, R Mitchell, and S Vidanovic. 2013. Energy Savings from Window Attachments. . Lawrence Berkeley National Laboratory, Berkeley, California. at: http://energy.gov/sites/prod/files/2013/11/f5/energy_savings_from_windows_attachments.pdf.

EIA. (2021). *Annual Energy Outlook 2021*. https://www.eia.gov/outlooks/aeo/

Foster, M., & Oreszczyn, T. (2001). Occupant control of passive systems: the use of Venetian blinds. *Building and Environment*, *36*(2), 149–155.

Huang, J., Hanford, J., & Yang, F. (1999). *Residential heating and cooling loads component analysis*. Building Technologies Department, Environmental Energy Technologies Division~….

Petersen, J. M., Sullivan, G., Cort, K. A., Metzger, C. E., & Merzouk, M. (2016). *Evaluation of Cellular Shades in the PNNL Lab Homes*. PNNL-24857 Rev 2. Pacific Northwest National Laboratory.

Rubin, A. I., Collins, B. L., & Tibbott, R. L. (1978). *Window blinds as a potential energy saver: A case study*. US Department of Commerce, National Bureau of Standards.

SparkFun. (2020). *HC-SR04 Ultrasonic Sensor Library*. GitHub. https://github.com/sparkfun/HC-SR04_UltrasonicSensor

Van Den Wymelenberg, K. (2012). Patterns of occupant interaction with window blinds: A literature review. *Energy and Buildings*, *51*, 165–176.

Appendix A

– Detailed Part List and Material Costs

Table A.1. Detailed material cost for the sill-mounted ultrasonic distance sensor installation.

Sill-Mounted Ultrasonic Distance Sensor					
Item Description	**Vendor**	**Part Number**	**Unit Cost ($)**	**Estimated Percentage Consumed (%)**	**Implemented Material Cost ($)**
Ultrasound-based distance sensor	Amazon	B01COSN7O6	$9.99	20.0%	$2.00
Semi-permanent breadboard	Amazon	B07ZYNWJ1S	$12.99	16.7%	$2.17
Ribbon cable for sensors	Amazon	B0775WHBP5	$9.99	25.0%	$2.50
Wood Trim	Home Depot	HDO142	$1.08	8.3%	$0.09
				Total Material Cost:	**$6.75**

Table A.2. Detailed material cost for the shade-mounted ultrasonic distance sensor installation.

Shade-Mounted Ultrasonic Distance Sensor					
Item Description	**Vendor**	**Part Number**	**Unit Cost ($)**	**Estimated Percentage Consumed (%)**	**Implemented Material Cost ($)**
Ultrasound-based distance sensor	Amazon	B01COSN7O6	$9.99	20.0%	$2.00
Semi-permanent breadboard	Amazon	B07ZYNWJ1S	$12.99	16.7%	$2.17
Ribbon cable for sensors	Amazon	B0775WHBP5	$9.99	25.0%	$2.50
Zip Ties	Home Depot	GT-200STCB	$7.98	5.0%	$0.40
				Total Material Cost:	**$7.06**

Table A.3. Detailed material cost for the sill-mounted infrared distance sensor installation.

Sill-Mounted Infrared Distance Sensor					
Item Description	**Vendor**	**Part Number**	**Unit Cost ($)**	**Estimated Percentage Consumed (%)**	**Implemented Material Cost ($)**
Laser-based distance sensor	Amazon	B08RRT1KJ6	$13.99	50.0%	$7.00
Semi-permanent breadboard	Amazon	B07ZYNWJ1S	$12.99	16.7%	$2.17

Sill-Mounted Infrared Distance Sensor					
Item Description	**Vendor**	**Part Number**	**Unit Cost ($)**	**Estimated Percentage Consumed (%)**	**Implemented Material Cost ($)**
Ribbon cable for sensors	Amazon	B0775WHBP5	$9.99	25.0%	$2.50
Wood Trim	Home Depot	HDO142	$1.08	8.3%	$0.09
				Total Material Cost:	**$11.75**

Table A.4. Detailed material cost for the shade-mounted infrared distance sensor installation.

Shade-Mounted Infrared Distance Sensor					
Item Description	**Vendor**	**Part Number**	**Unit Cost ($)**	**Estimated Percentage Consumed (%)**	**Implemented Material Cost ($)**
Laser-based distance sensor	Amazon	B08RRT1KJ6	$13.99	50.0%	$7.00
Semi-permanent breadboard	Amazon	B07ZYNWJ1S	$12.99	16.7%	$2.17
Ribbon cable for sensors	Amazon	B0775WHBP5	$9.99	25.0%	$2.50
Zip Ties	Home Depot	GT-200STCB	$7.98	5.0%	$0.40
				Total Material Cost:	**$12.06**

Table A.5. Detailed material cost for the Hall effect sensor array sensor installation.

Hall Effect Sensor Array					
Item Description	**Vendor**	**Part Number**	**Unit Cost ($)**	**Estimated Percentage Consumed (%)**	**Implemented Material Cost ($)**
Hall Effect Sensor	Amazon	B00SWK15ZE	$6.99	100.0%	$6.99
Semi-permanent breadboard	Amazon	B07ZYNWJ1S	$12.99	16.7%	$2.17
Ribbon cable for sensors	Amazon	B0775WHBP5	$9.99	25.0%	$2.50
Neodymium Magnet	Amazon	B07D8QPG2Y	$10.99	2.2%	$0.24
Zip Ties	Home Depot	GT-200STCB	$7.98	5.0%	$0.40
Wood Trim	Home Depot	HDO142	$1.08	600.0%	$6.48
				Total Material Cost:	**$18.78**

Table A.6. Detailed material cost for magnetic encoder strip sensor installation.

Magnetic Encoder Strip					
Item Description	**Vendor**	**Part Number**	**Unit Cost ($)**	**Estimated Percentage Consumed (%)**	**Implemented Material Cost ($)**
Magnetic linear encoder tape	Adafruit	4680	$47.50	200.0%	$95.00
Hall Effect Sensor	Amazon	B00SWK15ZE	$6.99	20.0%	$1.40
Semi-permanent breadboard	Amazon	B07ZYNWJ1S	$12.99	16.7%	$2.17
Ribbon cable for sensors	Amazon	B0775WHBP5	$9.99	25.0%	$2.50
Wood Trim	Home Depot	HDO142	$1.08	8.3%	$0.09
Zip Ties	Home Depot	GT-200STCB	$7.98	5.0%	$0.40
				Total Material Cost:	**$101.55**

Appendix B – HC-SR04 Ultrasonic Distance Sensor Pseudo-Code

Below is some pseudo-code for the HC-SR04 adopted from the Sparkfun Arduino library (SparkFun 2020):

```
######################
Initialize Echo_Pin, Trigger_Pin, Time_1, Time_2, Distance_cm,
Distance_in

Set Echo_Pin as Input
Set Trigger_Pin as Output

Begin Program
# Emitting Signal
Set Trigger_Pin High
Wait 10 microseconds
Set Trigger_Pin Low

# Receiving Signal
While(Echo_Pin == Low){
     Time_1 = Get_Current_Time()
}
While(Echo_Pin == High){
     Time_2 = Get_Current_Time()
}

# Calculating Distance. Constants found in HC-SR04 datasheet
# for the speed of sound in air at sea level.
Distance_in = (Time_2 - Time_1)/148.0

Print Distance_in

End Program
######################
```

Appendix C – Hall Effect Sensor Array Pseudo-Code

Below is some pseudo-code developed for the Hall effect sensor array sensing approach. This code displays an example with three sensors, but the code can be scaled depending on the number of interrupt channels available. Please note: This code requires interrupts, so the language and data acquisition platform this approach is implemented in must have a built-in interrupt service routine.

```
######################
Initialize Interrupt_Pin_1, Interrupt_Pin_2, Interrupt_Pin_3,
Current_Location
Current_Location = 0

Interrupt_1(){ # Interrupt for magnet passing Hall sensor 1
Set Current_Location = 0 # inches
}

Interrupt_2(){ # Interrupt for magnet passing Hall sensor 2
Set Current_Location = 6 # inches
}

Interrupt_3(){ # Interrupt for magnet passing Hall sensor 3
Set Current_Location = 12 # inches
}


Attach Interrupt_1 to Interrupt_Pin_1
Attach Interrupt_2 to Interrupt_Pin_2
Attach Interrupt_3 to Interrupt_Pin_3


Begin Program

Print Current_Location

End Program
######################
```

PNNL-32000

Pacific Northwest National Laboratory

902 Battelle Boulevard
P.O. Box 999
Richland, WA 99352
1-888-375-PNNL (7665)

www.pnnl.gov